Project Title: A Fundamental Study of Inorganic Clathrate and Other Open-Framework Materials

Project Period: 06/14/2004 – 06/14/2017

Project Budget: \$ 1,520,985

Recipient: University of South Florida

Address: 4202 E. Fowler Ave., Tampa, FL 33620

Award Number: DE-FG02-04ER46145

Contact: Ms. Mindy Owen, USF Sponsored Research, RSCH-awards@usf.edu, (813) 974-3679

Postal Address: Department of Physics, University of South Florida 4202 E. Fowler Ave.,

Tampa, FL 33620

Principal Investigator: Prof. George S. Nolas

DOE/Office of Science Program Office: Division of Materials Sciences and Engineering

DOE/Office of Science Program Technical Program Manager Contact: Dr. Bonnie Gersten

Summary

Clathrates are "open-structured" materials with a host framework that has the ability to encage guest atoms or molecules. There are many interesting physical properties observed in clathrates, including glass-like thermal conductivity, superconductivity in sp3 bonded solids, magnetism, and heavy atom tunneling in the crystalline state.[1] These physical properties are a direct consequence of their structural properties and make clathrates promising for a range of useful applications, from thermoelectrics to photovoltaics, as well as potentially ultra-hard materials. The key findings from this project that are described in detail below, in the Project Results and Discussion section, include:

- Optimized synthesis and structural properties of microcrystalline Na_xSi₁₃₆ clathrates.
- Synthesis of a new "open framework" phase, Na_{1-x}Ge_{3+z}, employing our synthetic approach.
- Crystal growth and transport properties measurements on single-crystal clathrates, for the first time, by employing Spark Plasma Sintering.
- Selective clathrate crystal growth by employing a process whereby reaction of the vapor phase with spatially separated graphite, in a closed volume, allows for control of Na vapor pressure: Kinetically Control Thermal Decomposition (KCTD).
- Used these techniques to synthesize and structurally characterize Na_xSi_{136} (0 < x < 24) single crystals for the first time.
- Measured the temperature-dependent transport properties of Na_xSi₁₃₆.
- Grew and characterized single crystals of K₈Si₄₆ and K₁₇Si₁₃₆.
- Selective synthesis of clathrates employing SPS by tuning the SPS parameters.
- Investigated the pressure effects on crystal size for SPS crystal growth.
- Si-Ge clathrate alloys synthesized for the first time by SPS and KCTD.
- Began an investigation into ionic liquid synthesis of clathrate compositions.
- Single crystal and microcrystalline Na₈Al₈Si₃₈ synthesized, for the first time, by KCTD and SPS by employing multiple precursors allowing for structure and transport properties investigations of Na₈Al₈Si₃₈.
- Simultaneous electrochemical redox and ion-exchange reactions: A new approach for inorganic clathrate synthesis and crystal growth.
- Quaternary clathrate-II Cs₈Na₁₆Al₂₄Si₁₁₂ synthesized by multi-precursor, ion-exchange reaction employing KCTD, and its low temperature transport properties measured, for the first time.
- Clathrate-II (K,Ba)₁₆(Ga,Sn)₁₃₆ compositions synthesized and densified into dense polycrystalline form employing SPS; structure and transport properties investigated.
- Type-II clathrate with a Li-Ge framework synthesized and characterized.
- Densified nanocrystals into dense polycrystalline solids with nano-scale grains via SPS for transport properties investigations.

Background

Due to formidable synthetic challenges, many materials of scientific and technological interest are first obtained as microcrystalline powders. High purity, high yield processing techniques are often lacking and thus care must be taken in interpretation of the observed structural, chemical, and physical properties of powder or polycrystalline materials, which can be strongly influenced by extrinsic properties. Furthermore, the preparation of high-quality single crystals for many materials by traditional techniques can be especially challenging in cases where the elemental constituents have greatly differing melting points and/or vapor pressures, when the desired compound is thermodynamically metastable, or where growth with participation of the melt is generally not possible. New processing techniques are therefore imperative in order to investigate the intrinsic properties of these materials and elucidate their fundamental physical properties.

Intermetallic clathrates constitute one such class of materials. The complex crystal structures of intermetallic clathrates are characterized by mainly group 14 host frameworks encapsulating guestions in polyhedral cages. The unique features of clathrate structures are intimately related to their physical properties, offering ideal systems for the study of structure-property relationships in crystalline solids. Moreover, intermetallic clathrates are being actively investigated due to their potential for application in thermoelectrics, photovoltaics and opto-electronics, superconductivity, and magnetocaloric technologies.

We have developed different processing techniques in order to synthesize phase-pure high yield clathrates reproducibly, as well as grow single crystals for the first time. We also employed these techniques to synthesize new "open-framework" compounds. These advances in materials processing and crystal growth allowed for the investigation of the physical properties of a variety of different clathrate compositions for the first time.

Introduction

Clathrates, or "open-framework" complexes are sometimes thought of as inclusion compounds. Several families of clathrates are known, the host lattices can be organic or inorganic. The most important and well-studied of these possess similar structure types as that of the clathrate hydrates,[1] where face-sharing polyhedra enclose guest species. Clathrate hydrates have been known for two centuries, whereas isostructural inorganic compounds, in which Si, Ge and Sn elements form the host lattice and alkali-metals, alkaline-earth or less-common metals are the guest species, have been more recently investigated. In all cases, tetrahedral bonding forms the framework, with guest species occupying the relatively large "voids" inside the polyhedral "cages".

A large majority of the characteristic polyhedral cages that form the framework of clathrate structures exhibit twelve pentagonal faces typically in combination with a lower number of polyhedra that contain hexagonal faces, according to Euler's rule for polyhedrons. The smallest and most frequent of these is the pentagonal dodecahedron, with only 12 pentagonal faces, 20 vertices and 30 edges, more simply referred to as 5^{12} , and continue in increasing size: $(5^{12}6^2)$, 3 $(5^{12}6^3)$, 4 $(5^{12}6^4)$ and 8 $(5^{12}6^8)$ hexagonal faces. Most of the known clathrate structure types are composed of a combination of two of these polyhedra that form large and highly symmetrical unit cells involving, for example, 46 or 136 atoms in the framework lattice for the clathrate-I and

clathrate-II structure types, respectively. Whatever the arrangement of these polyhedral cages, the host species are tetrahedrally bonded with similar bond angles, close to 108° pentagonal angles and 120° hexagonal angles. Clathrate host lattices can therefore be considered as open forms of tetrahedrally bonded structures. It should therefore come as no surprise that that clathrate analogues, clathrasils, also exist with silica as the host lattice as this is another well-known tetrahedrally bonded structure. In addition, most clathrate structures have a simple relationship with those of well-known metal alloys, such as the Cr₃Si and MgCu₂, in which the metal atoms are located on the same positions as the guest species inside the framework polyhedra would be, or where voids exist. Such alloys can therefore be thought of as templates for clathrate structures.

Another very interesting feature of clathrates is that the characteristic polyhedra, made of edge-sharing pentagonal and hexagonal faces, are related to the fullerene forms of carbon, the structures of which are based on the same geometrical rules. The C_{60} buckyball is formed by 12 pentagonal faces sharing edges with 20 hexagonal faces ($5^{12}6^{20}$). Clathrate polyhedra can be thought of as corresponding to the smallest possible fullerene clusters and form 3-D frameworks in order to neutralize the strains due to dangling bonds, whereas all the valence electrons are engaged in single or double bonds in a C_{60} buckyball enabling it to form isolated clusters. Due to their special cagelike architecture, and the relations they have with hydrates, clathrasils, inter-metallic alloys and fullerenes, the structures of inorganic clathrates are truly unique.

The inorganic clathrates Na_8Si_{46} and Na_xSi_{136} ($3\le x\le 11$) were discovered five decades ago, and their structures identified by comparison with those of the clathrate hydrates.[1, 2] Over the past two decades research on inorganic clathrates has intensified due to their unique structure-property relationships as well as their potential for energy-related applications, including thermoelectrics and photovoltaics.[1] Within this time period stardard synthetic approaches were employed in the preparation of compositions for investigation; however, it soon became clear that many compositions of interest were unattainable by traditional synthetic techniques.

Due to the efforts from several different research groups, and specifically the research under this project, substantial research has been undertaken resulting in a great deal of knowledge on these unique materials. Fundamental structure-property relationships have been revealed. In addition, certain compositions and structure types show promise for technological applications. Inorganic clathrate research is therefore a field of research that continues to be of interest to the scientific community. Given the current level of understanding in the field, there is no doubt that the research under this project resulted in extensive advances, if not the most important advances, in research on inorganic clathrates and an understanding of their transport properties.

Project Results and Discussion

High yield synthesis of microcrystalline clathrates

We prepared Na_xSi₁₃₆ clathrates via an optimized variant of the thermal decomposition ("flash degassing") technique of the Zintl compound Na₄Si₄ under vacuum in order that the physical properties of Na_xSi₁₃₆ clathrates be thoroughly characterized for the first time.[3] This approach was reproducible and resulted in high yield processing of microcrystalline specimens. We achieved this with a custom-designed furnace system that allowed for the synthesis of Na₂₄Si₁₃₆ in relatively large quantities without decomposition of the type II clathrate phase. Figure 1 illustrates the clathrate-II crystal structure. The Na content is then varied by further heating under vacuum at temperatures between 360 and 425°C, the temperature and duration of heating determining the final Na content. The synthesis was scaled to produce over one gram of high quality Na_xSi₁₃₆ (a ten-fold increase over previous results)[3] in a single synthesis run, resulting in enough material to begin a detailed structural analysis of these materials. This work revealed insight into the structural response of the lattice to Na filling for Na_xSi₁₃₆ the first time. As shown in Figure 2, at higher Na content (x > 8) increased filling results in an expansion of the structure; however, at lower Na content (x < 8) the lattice parameter decreases with increasing Na content. The results are linked to the relative occupation of the two distinct cages in the structure, as determined from Rietveld structural refinement results.[3] At lower Na contents (x < 8) only the larger Si₂₈ cage (8b site) is occupied, with the Si₂₀ (16c) sites being completely empty. The latter sites only begin to be occupied once the Si₂₈ cages are full. This indicates that Na preferentially occupies the Si₂₀ cages for x < 24. Thus filling of the smaller Si₂₀ cages (for x > 8) results in an expansion of the structure, while filling of only the larger Si₂₈ cages (x < 8) results in a slight but clear shrinking of the structure. This is the first unequivocal experimental evidence of this effect in group 14 clathrate-II materials, and is due to particular electrostatic interactions between guest and cage as well as charge transfer from guest to framework. This result indicates the compositions thus far investigated contain Na inside the Si₂₈ hexakaidecahedra and further corroborates the dynamic disorder, or "rattling", nature of Na inside the large hexakaidecahedra formed by Si. This structural analysis plays an important role in correlation with the physical properties of these Na_xSi₁₃₆ in the complete Na range of compositions ($0 \le x \le 24$), as will be described below.

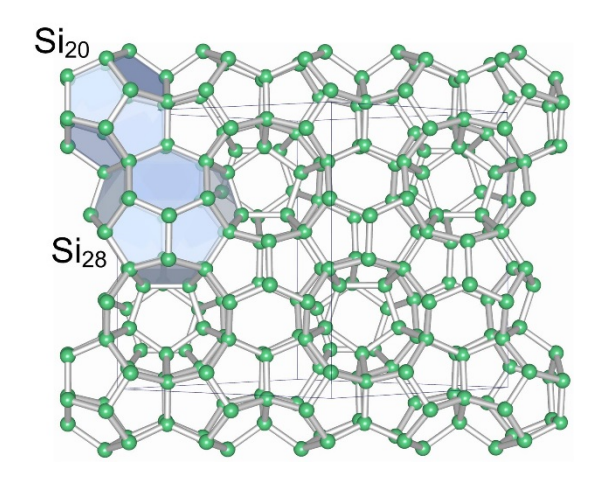


Figure 1. The cubic (space group $Fd\overline{3}m$) silicon clathrate-II framework, Si(cF136). The two silicon cages that can be occupied by Na are highlighted in the upper left.

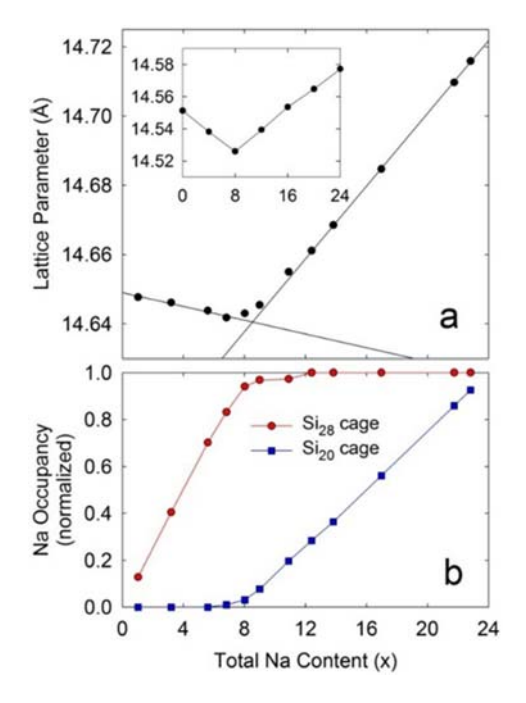


Figure 2. (a) Experimental normalized cage occupancies for Na@Si₂₀ and Na@Si₂₈ and (b) experimental cubic unit cell parameters, both as a function of total Na content. Inset (same units as main figure): Theoretical lattice parameters obtained from density functional theory calculations.

Ternary and quaternary clathrates, including framework substitution, were synthesized and characterized. We demonstrated that transition metals such as Ag [4] and Cu [5] can be substituted for Ge on the framework of ternary clathrate-II compounds such as Cs₈Na₁₆Ge₁₃₆. Our single crystal X-ray diffraction studies [4] of Cs₈Na₁₆Ag_yGe_{136-y} revealed that this substitution preferentially occurs at the 96g framework site. This is likely linked to the local symmetry of this site, supporting the most "distorted" bonding geometry in the framework, as this has the highest number of unequal bond angles, and also the largest deviation (~ 120°) from the "ideal" tetrahedral bond angle of 109.5°.[4] In addition, our work on Cu substitution for Ge in Cs₈Na₁₆Ge₁₃₆ was shown to influence the transport properties of this material (Figure 3).[5] We note these Ge-based materials are readily densified employing standard techniques such as hot pressing, unlike Na_xSi₁₃₆.[3] The electrical transport of Cs₈Na₁₆Cu_yGe_{136-y} clathrates is indicative of behavior typical of a metallic or heavily doped semiconductor material. This can be qualitatively understood in terms of a simplified "rigid band" model, in which the alkali guests (Cs and Na) donate electrons to the Ge and Ge-Cu framework conduction bands resulting in a relatively high concentration of carriers.[6] Hall measurements indicate electrons to be the majority carriers. The four-coordinated covalent bonding in the Ge₁₃₆ framework is analogous to the sp³ bonding found in elemental diamond structure Ge, in which substitutional Cu has been shown to behave as an electronic acceptor. [7] Our data are consistent with that found in the diamond structured analogue, indicating

partial charge compensation as a result of Cu substitution on the Ge framework.[5] The thermal conductivities of the two specimens show very similar temperature dependences, as expected since a considerable electronic contribution to the thermal conductivity is expected. We note that semiconducting filled type II clathrates are in general expected to possess relatively low lattice thermal conductivity, κ_L , due to their enlarged unit cell and potential phonon scattering as a result of large amplitude anharmonic guest atom vibrations.[1, 4, 6, 8]

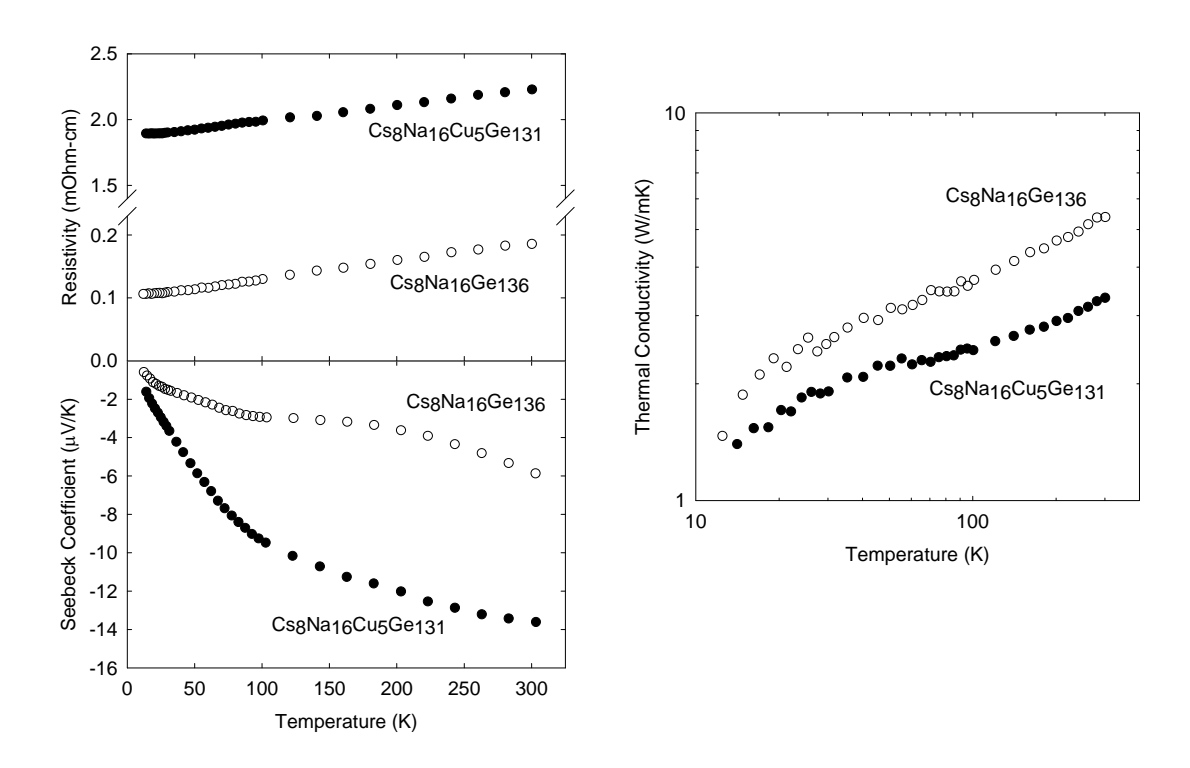


Figure 3. Temperature dependence of the electrical resistivity and Seebeck coefficient (left) and thermal conductivity (right) for Cs₈Na₁₆Ge₁₃₆ (open symbols) and Cs₈Na₁₆Cu₅Ge₁₃₁ (filled symbols).

The discovery of a new binary framework phase, Na_{1-x}Ge_{3+z}, prepared by the new thermal decomposition of the binary Zintl phase Na₄Ge₄ was also achieved.[9, 10] The crystal structure is illustrated in Figure 4, and represents a new crystalline binary phase in the Na–Ge material system that had not previously been synthesized nor its crystal structure determined.[9] The hexagonal structure contains a covalently bonded framework of Ge atoms that form channels along the *c*-direction that encapsulate Na, akin to the channels found in some oxide zeolites. Transport measurements showed relatively large room temperature resistivity (of the order of 1 Ohm-m) and thermopower (– 380 μ V/K) with a very low thermal conductivity (< 0.7W/mK at and below room temperature). This phase was very recently reproduced, and the structural features verified, by a high pressure synthesis approach in collaboration with the Carnegie Institute of Science.[11]

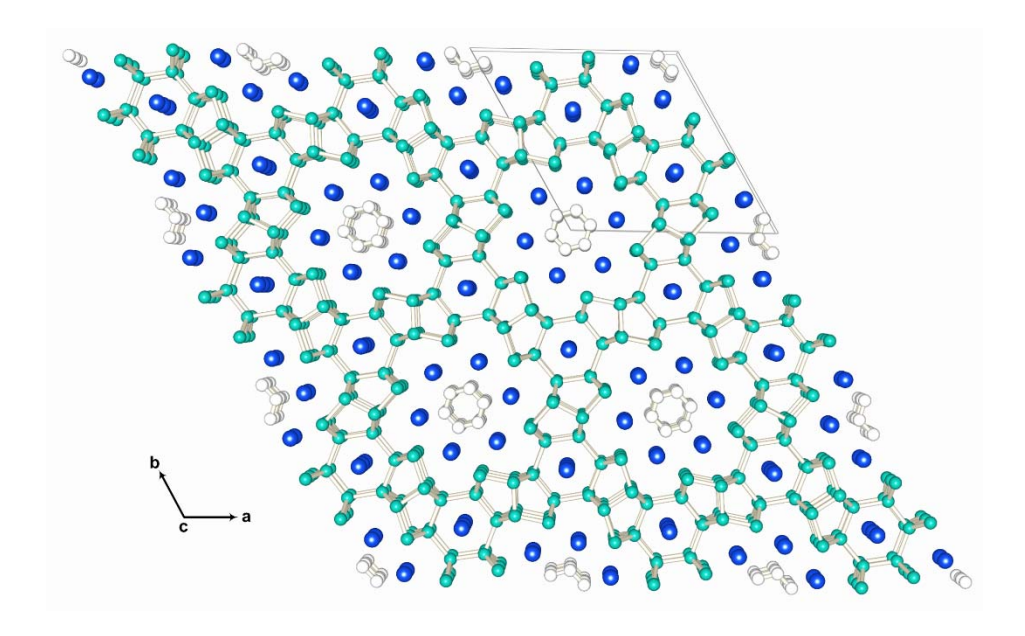


Figure 4. Crystal structure of the new zeolite-like framework phase, $Na_{1-x}Ge_{3+z}$, viewed down the *c*-axis. Na are represented by the blue circles and Ge by green and open circles. The six Ge atoms at the center of the channels represent six equivalent positions where one Ge atom may reside.

Clathrate crystal growth via Spark Plasma Sintering

The spark plasma sintering (SPS) technique, a variant of field-assisted processing, has in little more than a decade become an established consolidation method for fabrication of dense polycrystalline specimens. Pulsed DC electrical current is sourced through the specimen and die from the bottom electrode to the top electrode, which simultaneously act as the means for application of uniaxial pressure to the powder specimen. We demonstrated the effective use of SPS processing, as illustrated in Figure 5, for crystal growth of the intermetallic clathrate-II Na₂₄Si₁₃₆,[12] for which no route for single crystal preparation had been previously identified. Na_{24-x}Si₁₃₆ was the first intermetallic clathrate reported more than four decades ago, [2] however, until this work no method for single crystal growth of this material had been identified.[1] The process is driven by the electric field that is present during the SPS process and the formation and evaporation of Na formed at the cathode. We propose that Na₂₄Si₁₃₆ forms by oxidation of Si₄⁴⁻ at the anode (bottom electrode), whereas sodium is reduced at the cathode (top electrode). Upon oxidation of the Si4⁴⁻ cluster anions in Na4Si4, the clathrate framework is formed, while simultaneously encapsulating sodium in the resulting Si₂₀ and Si₂₈ cavities of the silicon framework. The yield of Na₂₄Si₁₃₆ crystals in the bottom portion of the compact increase as the reaction is allowed to progress for longer durations of time (Figures 6b and 6a). The observations shown in Figure 6 clearly suggest an influence of the DC electrical current. We propose that Na₂₄Si₁₃₆ forms by oxidation of Si⁴⁻ at the anode (bottom electrode), whereas sodium is reduced at the cathode (top electrode).

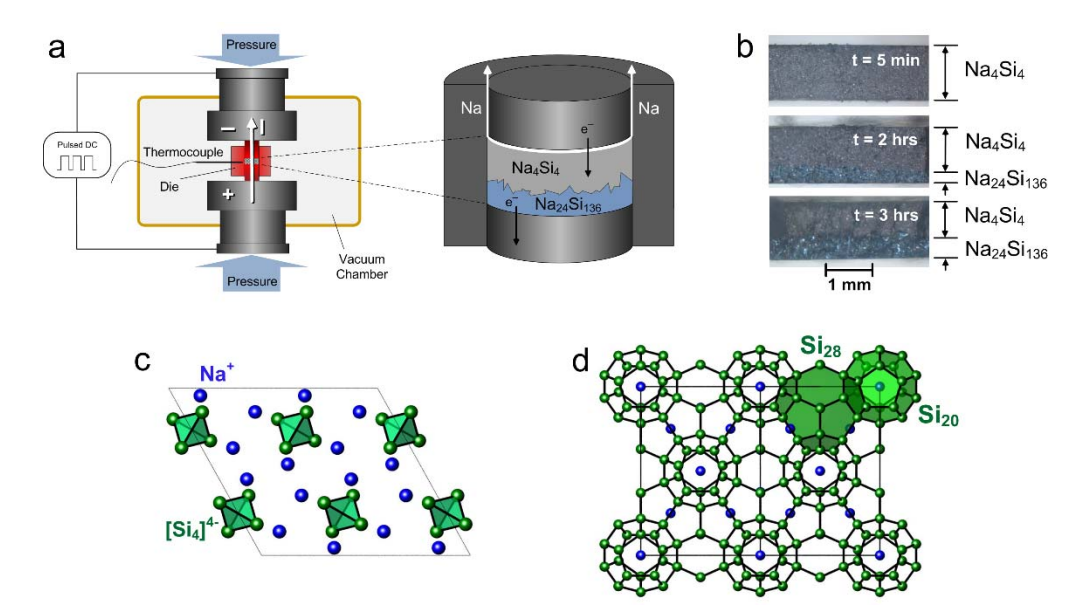
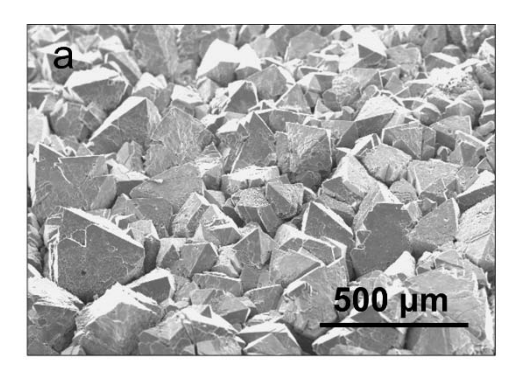


Figure 5 (a) Schematic of the spark plasma sintering (SPS) setup used for Na₂₄Si₁₃₆ crystal growth, with polarity of the applied voltage indicated. (b) Cross-sections of SPS-treated specimens, reacted at 600 °C and 100 MPa for 5 minutes, 2 hours, and 3 hours, as indicated. The upper portion consists of Na₄Si₄ while the lower, bluish crystalline fraction is clathrate-II Na₂₄Si₁₃₆. (c) Crystal structure of the Na₄Si₄ precursor. (d) Crystal structure of the clathrate-II Na₂₄Si₁₃₆. Oxidation of Na₄Si₄ promotes formation of the Na₂₄Si₁₃₆ clathrate, and the Si₂₀ and Si₂₈ coordination polyhedrons of the clathrate are highlighted.



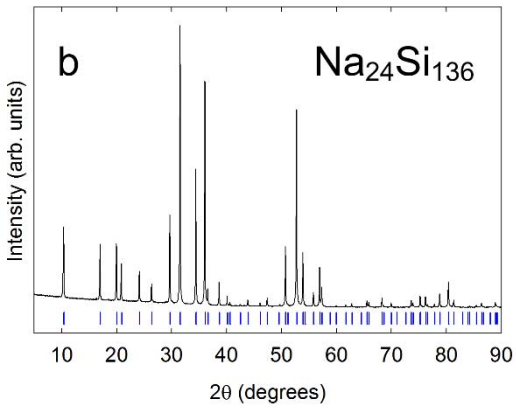


Figure 6 (a) Scanning electron microscope (SEM) secondary electron image of Na₂₄Si₁₃₆ crystals, after removal of residual Na₄Si₄ precursor by hydrolysis and dissolution. (b) Powder X-ray diffraction pattern for Na₂₄Si₁₃₆ grown at 600°C after removal of residual Na₄Si₄. All reflections correspond to Na₂₄Si₁₃₆, as illustrated by blue tick marks representing calculated reflection positions.

The PXRD pattern for a specimen ground from the $Na_{24}Si_{136}$ product is shown in Figure 6b, corroborating the phase purity of the specimen. All reflections are indexed with the clathrate-II crystal structure (space group $Fd\overline{3}m$, blue tick marks). The demonstrated synthesis of $Na_{24}Si_{136}$ by SPS thus constitutes a solution to a long standing challenge in the preparation of Na_xSi_{136} clathrates: the previously known Na_xSi_{136} synthetic routes, such as thermal decomposition or chemical oxidation of Na_4Si_4 , always produce the Na_8Si_{46} clathrate in significant amounts.[13-15] This secondary phase is very difficult to avoid in the products from these synthetic routes. α -Si is also a common impurity phase in such specimens.[13-15] Several runs demonstrated that $Na_{24}Si_{136}$ is reproducibly prepared by SPS as single phase specimens.

The electronic structure of the silicon clathrate-II compositions have received considerable theoretical attention [16-19] in an effort to understand the influence of Na loading of the framework polyhedral cages on the electronic properties of this system. Electrical properties have been inferred from measurements on microcrystalline specimens,[20-21] but achieving a fundamental understanding of the conduction in these materials, and their physical properties more generally, has until now remained elusive.[22] Our preparation of Na₂₄Si₁₃₆ single crystals has allowed for structural and physical properties investigations on single crystal Na₂₄Si₁₃₆ clathrates for the first time.[23] Heat capacity was measured on single crystal specimens, and temperature dependent four-probe electrical resistivity, Seebeck coefficient, and steady-state thermal conductivity measurements were carried out by our custom designed and built closed-cycle helium cryostat [24]. The transport data were reproduced on several crystals. The temperature dependence showed excellent repeatability, and the magnitude agreed within the estimated relative uncertainty of associated with the determination of the geometrical factor for the crystals.

Single-crystal X-ray diffraction studies indicated an exceptionally large atomic displacement parameter (U_{eq}) obtained for Na (8b site) in the Si₂₈ cage (denoted hereafter as Na@Si₂₈) is suggestive of large amplitude thermal motion, or 'rattling,' for this Na guest within its oversized Si₂₈ cage. Assuming a harmonic oscillator model (representing an Einstein mode associated with the Na guest), an estimate of the vibrational frequency, v, can be obtained [25] from the room temperature $U_{eq} = 0.110(2)$ Å², and the relation $U_{eq} = k_B T/[m(2\pi v)^2]$. Here k_B is Boltzmann's constant, m is the mass of the Na atom, and T = 293 K. Applying this model, a characteristic Einstein temperature $\Theta_E = hv/k_B$, where h is Planck's constant, of 75 K is inferred using U_{eq} for Na@Si₂₈ when centered at the 8b site. Though this value of Θ_E is interpreted only as an estimate, it evidences the presence of a low-frequency phonon mode associated with the Na@Si₂₈ guest. Vibrational modes are more conclusively observed from the measured specific heat, where the presence of these entropic degrees of freedom is apparent.

The measured specific heat $C_p(T)$ for Na₂₄Si₁₃₆ is shown in Figure 7. Plotting the data as C_p/T^3 vs. T reveals clear evidence of low energy Einstein mode contributions to the specific heat. The data (Figure 7) reveals clear evidence of low energy Einstein mode contributions to C_p , which appear as a peak in the temperature dependence in this representation.[26] Considering the contributions to C_p that are expected to be significant in this temperature range [27], a model comprised of a linear combination of terms was fit to $C_p = C_e + C_{E1} + C_{E2} + C_D$ where $C_e = \gamma T$ is the electronic heat capacity, γ is the Sommerfeld coefficient,

$$C_{Ei}(T) = 3N_{Ei}R \left(\frac{\Theta_{Ei}}{T}\right)^{2} \frac{\exp(\Theta_{Ei}/T)}{(\exp(\Theta_{Ei}/T) - 1)^{2}} \quad \text{and} \quad C_{D}(T) = 9N_{D}R \left(\frac{T}{\Theta_{D}}\right)^{3} \int_{0}^{\Theta_{D}/T} \frac{x^{4}e^{x}}{(e^{x} - 1)^{2}} dx$$

Here $N_{\rm Ei}$ and $\Theta_{\rm Ei}$ are the number (per formula unit) and Einstein temperature of oscillator i, respectively, and $\Theta_{\rm D}$ is the apparent Debye temperature. The key aspect to note from this analysis, although several illuminating aspects were revealed,[23] is the analyses confirm the presence of a low energy Einstein-like mode (= 55 K) clearly associated with the eight Na@Si28 guests per formula unit. This $\Theta_{\rm E1}$ determined from $C_{\rm P}$ data is lower than that obtained from $U_{\rm eq}$ above, possibly corroborating the additional dynamic disorder. Nevertheless the frequency of this "rattle" mode falls well inside the frequency range of the host Si₁₃₆ acoustic phonon branches predicted from density functional theory calculations [28] indicating the potential for a resonant phonon interaction, analogous to clathrate-I materials.[29, 30] The value $\gamma = 0.163(4)$ JK-2mol-1, determined from linear fits below 4 K in Figure 7, reflects a considerable electronic contribution to the specific heat and a substantial electronic density of states at the Fermi level typical of a metallic compound. This agrees with density functional calculations [31] for Na₂₄Si₁₃₆ which predict the Fermi level to coincide with a prominent peak in the electronic density of states, and also corroborates our metallic transport properties measurements.[23]

Observation of intrinsic electronic transport in Na-Si clathrates has been previously obscured by extrinsic effects originating in the microcrystalline nature of the specimens.[20, 22] The temperature dependent electrical resistivity, $\rho(T)$, data (Figure 8a) reveal metallic conduction, with ρ for the crystal reaching the value 0.03 m Ω -cm at 300 K. The Seebeck coefficient, S, (Figure 8a) reaches the value $-5~\mu\text{V/K}$ at room temperature, consistent with a high density of electrons as the majority carriers and further corroborating metallic conduction.

At the lowest temperature of our measurement, 12 K, $d\rho/dT > 0$ indicating the residual resistivity for the specimen has still not yet been reached. Although a value for the residual resistance ratio (RRR) incorporating data from lower temperatures will be larger, we calculate from our data a RRR of $\rho(300 \text{ K})/\rho(12 \text{ K}) = 14$. To our knowledge, this value is several times larger than the highest RRR values reported before our research to this point for known metallic clathrates (i.e. with $d\rho/dT$ positive definite), including both polycrystalline [32] and single crystal clathrate-I specimens [33]. The relatively high RRR value for the Na₂₄Si₁₃₆ specimen, taken together with the above inferred mobility, is further indication of both the high quality of the crystal and the pronounced metallic conduction.

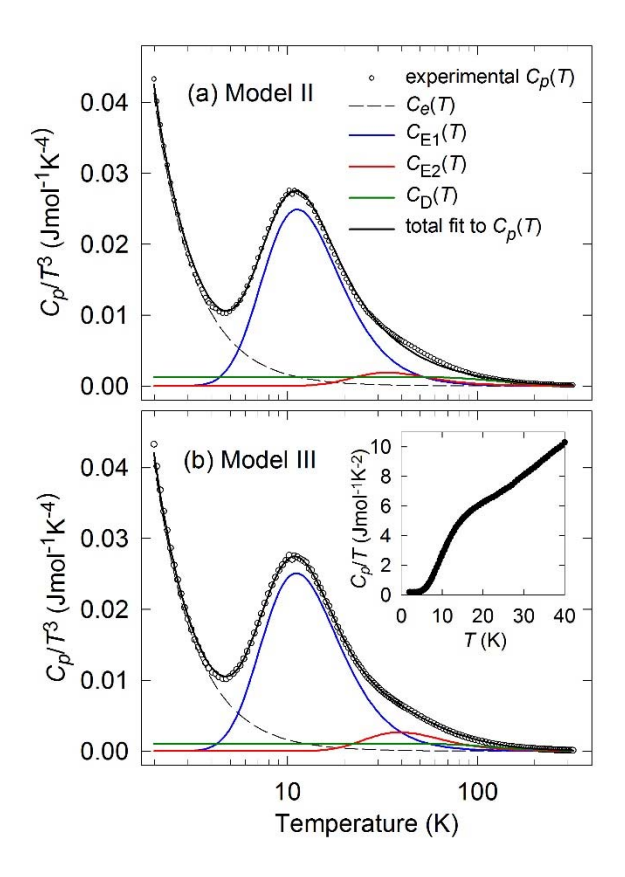


Figure 7 (a) Specific heat capacity of Na₂₄Si₁₃₆ plotted as C_p/T^3 against T, along with fits obtained with (a) Model II and (b) Model III described in Table I. Individual contributions to the overall fit are also shown as indicated. Inset to (b): The same experimental C_p data plotted as C_p/T against T, in the temperature range 0 to 40 K.

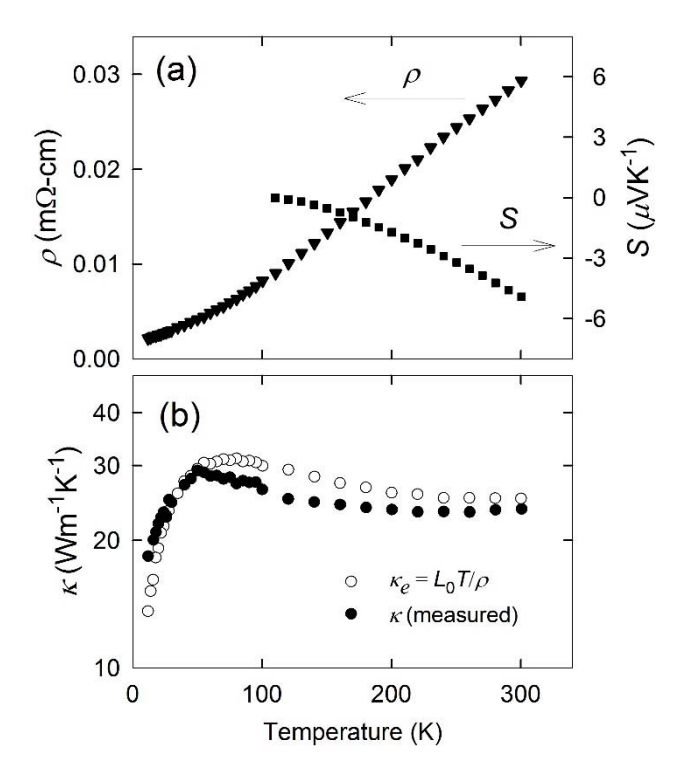


Figure 8 (a) Electrical resistivity (ρ) and Seebeck coefficient (S) of Na₂₄Si₁₃₆. (b) Thermal conductivity (κ) of Na₂₄Si₁₃₆ (closed symbols) and calculated contribution (open symbols) estimated from the Wiedemann-Franz relation.

The thermal conductivity, κ , of Na₂₄Si₁₃₆ (Figure 8b) is relatively large in comparison to other intermetallic clathrates. Indeed, the observed κ of Na₂₄Si₁₃₆ is substantially larger than previously observed for any intermetallic clathrate composition. Considering the pronounced metallic character observed in both C_p and ρ , a sizeable electronic contribution, κ_e , to the thermal conduction is expected. In a first approximation, employing the Wiedemann-Franz relation $\kappa_e = L_0 T/\rho$, with a temperature independent Lorentz number $L_0 = 2.45 \times 10^{-8} \text{ V}^2\text{s}^{-2}$ and the measured ρ , (Figure 8a) an estimate of κ_e is plotted in Figure 8b along with the experimentally measured thermal conductivity. Considering the low κ of the empty Si₁₃₆ framework,[34] the presence of the low energy Einstein-like 'rattle' mode clearly observed in the measured specific heat and discussed above, and the considerable expected electron-phonon scattering in light of the high density of conduction electrons, it is reasonable to conclude that κ_L of Na₂₄Si₁₃₆ is very low in this composition compared to the large κ_e component.

Kinetically Controlled Thermal Decomposition (KCTD)

We have introduced and optimized a novel method for the selective synthesis of single-crystal clathrate-I Na₈Si₄₆ and clathrate-II Na₂₄Si₁₃₆ for the first time.[35] The alkali metal was slowly removed from the Na₄Si₄ precursor by reaction of the vapor phase with spatially separated graphite, in an effectively closed volume under uniaxial pressure. We named this new and unique process Kinetically Control Thermal Decomposition.[35] This resulted in the single-crystal structure refinement for Na₈Si₄₆ for the first time.[36] In both phases, full occupation of all Si framework sites was observed, and both cages in the two clathrate structures were found to be fully occupied by the Na guests confirming stoichiometric compositions. Substantial disorder (large isotropic atomic displacement parameters, U_{eq}) is observed for the guest Na inside Si₂₈ in Na₂₄Si₁₃₆, in agreement with the "rattling" phonon mode and off-centering associated with this guest Na ion.

In our new KCTD processing technique, alkali metal is removed from the Na₄Si₄ precursor by reaction of the vapor phase with spatially separated graphite in an effectively closed volume under uniaxial pressure (Figure 9). A customized reaction vessel comprising a simple graphite punch and die design was constructed such that uniaxial pressure was applied to the specimen while heated in a tube furnace. To prevent the adhesion between graphite and clathrate crystals, a 1 mm thick layer of dry NaCl powder is introduced between the Na₄Si₄ precursor and graphite. The NaCl layer serves as an effective passive physical barrier to direct reaction between graphite and Na₄Si₄, but allows diffusive exchange of Na *via* the vapor phase. This C-NaCl-Na₄Si₄-NaCl-C "sandwich" is encapsulated on all sides by graphite foil to impede the escape of Na vapor, then compressed and clamped under uniaxial pressure of 115 MPa at room temperature. The entire assembly is introduced into a fused silica ampoule, coupled to a vacuum system, evacuated to 10⁻⁶ torr, and heated at the desired reaction temperature under dynamic vacuum.

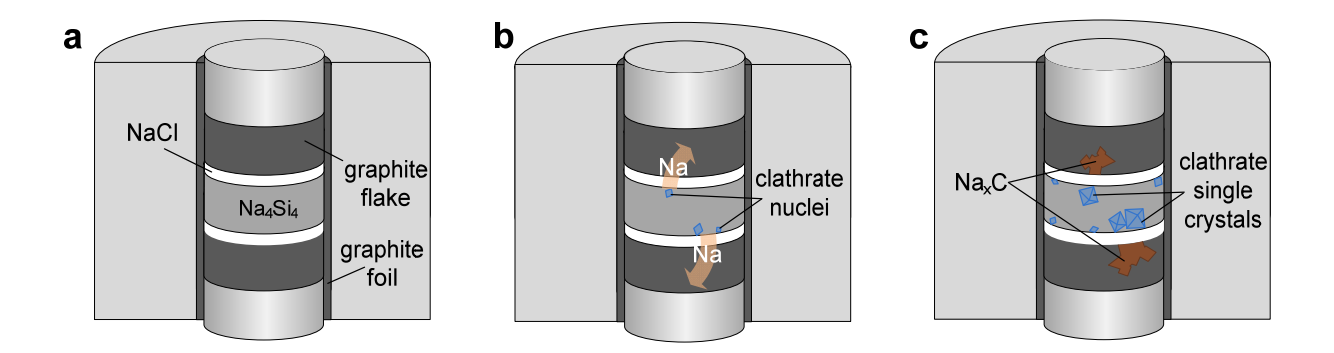


Figure 9. Simple schematic illustrating the Na₈Si₄₆ and Na₂₄Si₁₃₆ crystal growth processes. (a) The initial precursor configuration under uniaxial pressure in the punch and die. (b) Local composition change and nucleation of the clathrate phase. (c) Formation of intercalated graphite and clathrate crystal growth.[35]

The Na vapor, released from the Na₄Si₄ precursor, reacts with the spatially separated graphite, forming intercalation compounds Na_xC. Powder X-ray diffraction of the graphite flake recovered after the reaction confirms the presence of a mixture of stages of Na intercalated graphite. Presumably, the vapor pressure of Na over the intercalated graphite is less than that over Na₄Si₄, such that the intercalation of the graphite results in further release of Na from the precursor in order to locally maintain the Na vapor pressure over the precursor (le Chatelier's principle). Continued reaction to form Na_xC continuously drives the composition in the precursor Si rich. Nucleation of the respective clathrate phase ensues as the Na content of the sintered body is reduced, and the continuously applied uniaxial pressure facilitates mass transport between precursor and growing crystal. The rate of these dynamic processes is expected to be limited by mass exchange through the vapor phase, as well as diffusion of Na out of the precursor and the reaction kinetics of Na_xC formation.

This approach allowed for selectivity in crystal growth of Na₈Si₄₆ or Na₂₄Si₁₃₆ by merely changing the reaction temperature (Figure 10). Between 580 °C and 590 °C, clathrate-I Na₈Si₄₆ was found to exclusively form, whereas between 660 °C and 670 °C crystal growth of clathrate-II Na₂₄Si₁₃₆ occurred instead.[35] It is noteworthy that direct synthesis and crystal growth of these phases from the elements is unsuccessful, and the available Na-Si equilibrium diagram describes only a eutectic between Na₄Si₄ and Si and the absence of the clathrate phases.[37] Our manuscript describes in detail this approach, as well as the structural data and analyses from single-crystal XRD.[35] Of particular note is the RRR = 36 measured for Na₈Si₄₆ that is several times larger than the highest RRR value previously or since reported for any clathrate compositions, and is evidence of the high quality crystals grown by KCTD.

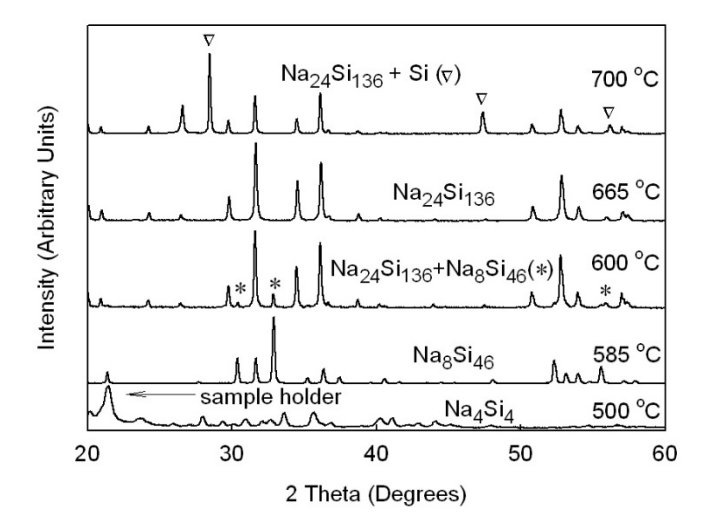


Figure 10. Formation of different phases at different temperatures starting from the same precursor Na₄Si₄. The single-crystal products were crushed in order to perform powder X-ray diffraction (XRD).

Single-crystal XRD studies and transport properties measurements on several different crystals of Na₈Si₄₆ and Na₂₄Si₁₃₆ resulted in the detailed investigation of the structure and bonding of these materials, their intrinsic low temperature properties, as well as an indication of the reproducibility of our two crystal-growth techniques.[12, 23, 35, 36] The intrinsic properties of both clathrate compositions were revealed for the first time through these analyses. Na₂₄Si₁₃₆ is perhaps the best example to illustrate our data and results. The harmonic oscillator model provides a simple yet

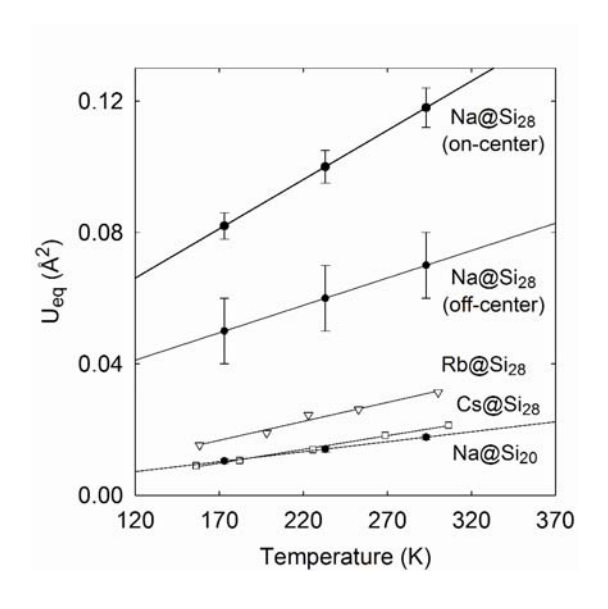


Figure 11. Temperature dependence of the Na U_{eq} obtained from single-crystal XRD, along with those of Cs@Si₂₈ and Rb@Si₂₈. Error bars represent one estimated standard deviation.[38]

useful tool to gain insight from atomic displacement parameter analysis,[25] especially for atomic vibrations that can be approximated by localized Einstein modes. At temperatures such that the Einstein temperature $\Theta_E = hv/k_B < 2T$, where v is the oscillator frequency, h is the Planck constant, and k_B is the Boltzmann constant, the simple classical relation $U_{eq}(T) = k_B T/[m(2\pi v)^2]$ can be expected to describe the temperature dependence of the atomic displacement parameter.[25] Fitting the data to this model as shown in Figure 11, we obtain estimated oscillator energies hv of

7.2 meV and 16.0 meV for Na@Si₂₈ and Na@Si₂₀, respectively. These results corroborate our inelastic neutron scattering measurements on microcrystalline powders.[38] The value for Na@Si₂₈ is indicative of a low-energy phonon mode associated with Na, and is comparable to rattler energies observed in clathrate-I compounds.[29] A substantial zero-temperature intercept of U_{eq} for Na at the 8b site (Na@Si₂₈) suggests static disorder. An off-centered (positioned at the 32e site, i.e. 4-fold split-site) model [39] was also refined against the single-crystal data. This was corroborated by our extensive powder XRD [35] and x-ray absorption spectroscopic [40] analyses. Although reduced in magnitude, U_{eq} remain relatively large even with the added static disorder. Model density functional theory investigations suggest either a flat, broad potential for Na in the Si₂₈ cage with the minimum in the cage center [31], or a very shallow minimum at approximately 0.5-1.0 Å away from the center.[41] In either case, at elevated temperatures thermal excitation will cause Na to dynamically explore the large volume of the Si₂₈ cage, in agreement with the strong temperature dependence of U_{eq} for Na@Si₂₈.[38]

The intrinsic transport properties measured on single-crystals of Na₂₄Si₁₃₆ grown by SPS,[23] and single-crystals of Na₈Si₄₆ and Na₂₄Si₁₃₆ grown from KCTD [35, 36, 38] serve to illustrate some of the capabilities now available through the use of these two synthetic approaches for the preparation, crystal growth and physical properties characterization of intermetallic clathrates. The key aspect of this work, however, is not only in overcoming the extrinsic effects that were previously unavoidable when consolidating microcrystalline specimens of these compositions, but in the fact that these synthetic approaches affords us the ability to explore key physical concepts associated with the structure-property relationships in intermetallic clathrate materials of differing compositions and "guest" concentrations. The availability of single crystals allows for such exploratory research. In addition, other new and novel materials can by prepared by one or both of these approaches, allowing for the further investigation into compositions with unique properties. An investigation into the structural and transport properties of a series of Na_xSi₁₃₆ specimens is one example.[42]

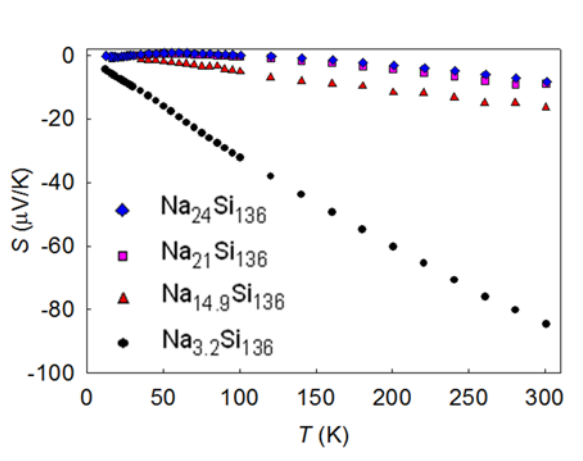


Figure 12. Temperature dependent S, ρ and κ for Na_xSi₁₃₆ compositions with different Na concentrations, x.

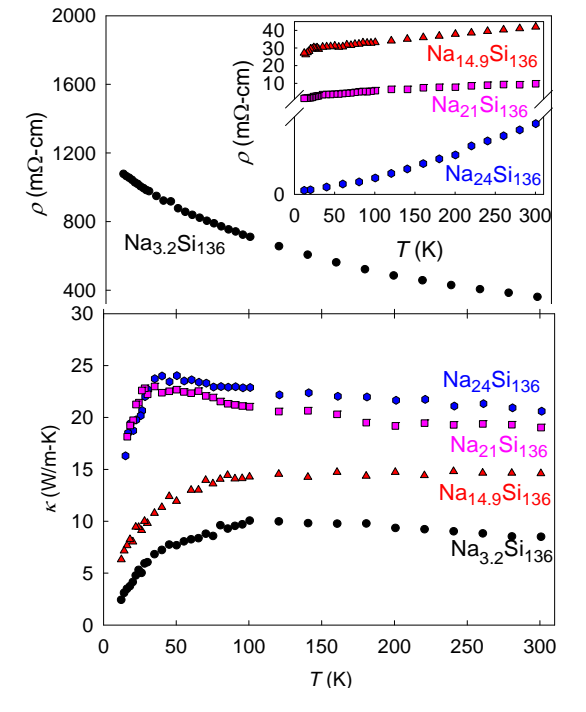


Figure 12 shows the temperature dependence of ρ , S and κ for Na_xSi₁₃₆. The modulus of S increases with temperature, as expected in metals and heavily doped semiconductors with negligible phonon drag. The relatively low magnitude of S for Na₂₄Si₁₃₆ is typical for metals where the location of the Fermi level is well inside the conduction band, as indicated by density-functional theory calculations.[31, 43] As the Na content decreases, the modulus of S increases, reaching a value of 85 μ V/K at room temperature for Na_{2.9}Si₁₃₆. According to these theoretical studies, the similarity between the density of states profiles for Na (both 3s and 3p) and the total density of states indicates a significant hybridization between metallic Na and the Si framework wavefunctions when Si₂₀ are filled. This is consistent with the metallic behavior of Na_xSi₁₃₆ for high Na loading. The average Na₁-Si and Na₂-Si distances decrease as x decreases to 8.2 (Na₁ being Na@Si₂₀ and Na₂ Na@Si₂₈). This may imply a significant hybridization between Na and Si corroborating the metallic behavior for x > 8. For x < 8 however, there are no Na₁ which presumably would reduce hybridization.

The temperature dependence of ρ indicates an apparent metal-to-semiconductor transition (Figure 12). There is a clear difference in the magnitude and temperature dependence of ρ as x changes from 2.9 to 24. The ρ values increase with increasing temperature for x = 8.2, 14.7 and 24, typical for metals, and decrease with increasing temperature for x = 2.9 and 5.1, typical for semimetallic or semiconducting materials. The room temperature ρ value for Na_{2.9}Si₁₃₆ is over two orders of magnitude higher than that for Na_{14.7}Si₁₃₆, and five orders of magnitude lower than that of the lowest Na content Na_xSi₁₃₆ specimens hot pressed from powders.[2, 43] From Quantum Molecular Dynamics studies on Si₁₃₆ and Na₄Si₁₃₆ it was shown that Na moves away from the center of Si₂₈ by 0.17 Å.[44] From EXAFS studies on Na₈Si₁₃₆[39] a strong interaction between Na₂ results in Jahn-Teller distortion and Na₂ dimmer formation, possibly originating from the spin-spin interactions from the unpaired 3s electrons of Na. Our results show that the Na2-Na2 distances decrease as x decreases. The shortest Na2-Na2 distance for Na₂₄Si₁₃₆ is 6.01 Å and decreases to 5.90 Å for Na_{2.9}Si₁₃₆; therefore, partial covalent bonding between Na₂ is more likely to occur at low Na concentrations. This partial covalent bonding between Na2, combined with the weak Na2-Si hybridization that results from the larger Na2-Si distances for x < 8, [39, 40, 43] may result in localization of the electrons and 'drive' the system to a less metallic state. Similar behavior in the endohedral metallofullerene Y@C₈₂ has been reported.[45] Our experimental results corroborate prior theoretical work. Semiconducting behavior for Na₄Si₁₃₆ was predicted by the first principle full-potential all electron linearized plane wave method.[35] It was suggested that the Jahn-Teller effect lifts the degeneracy at the Γ point and opens a small band gap.[35] In addition, Mott [20] argued that the Na wavefunction overlap decreases as the Na concentration decreases, and the electrons become localized on the Na atoms. When this localization occurs, a Mott transition takes place and the system becomes semiconducting. [20] This is corroborated by the increase in the Na-Si distances for x < 8. As Na moves away from the Si framework atoms, there may be less hybridization between Na and Si which results in localization of the electrons around Na. The shortest Na-Na distance (5.1759 Å) excludes the possibility of direct Na-Na interaction, as also suggested by Roy et al. [20] The metal-insulator transition with Na content can clearly be seen from Figure 13.

The thermal conductivities for the five Na_xSi_{136} specimens are also shown in Figure 12. The magnitude of κ is relatively large as compared to that of other intermetallic clathrates.[1, 46] The observed κ for Na_24Si_{136} is higher than the other clathrates shown in Figure 12 due to the fact that

it is dominated by the electronic component.[23] The room temperature values of κ for Na_{2.9}Si₁₃₆ and Na_{5.1}Si₁₃₆, the two specimens with the lowest Na content, are approximately three times lower than that of Na₂₄Si₁₃₆.

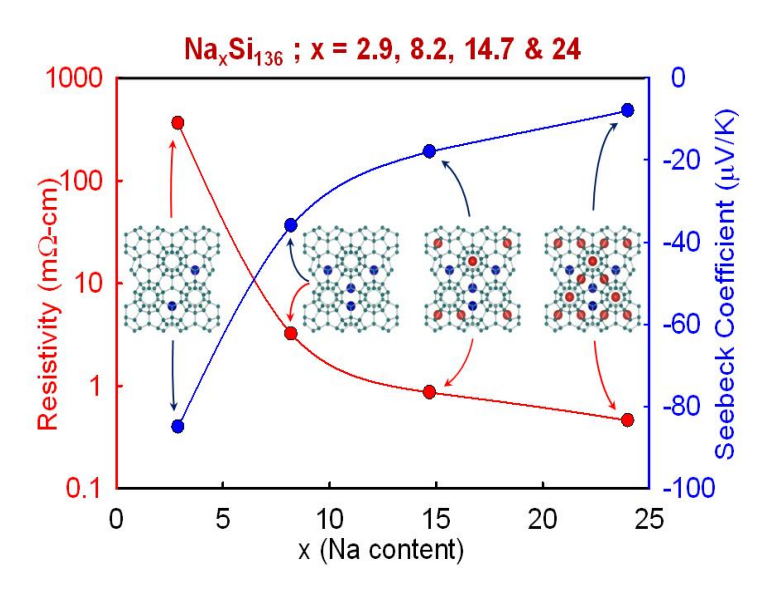


Figure 13. Room temperature S and ρ as a function of Na content, x, clearly showing the metalinsulator transition with Na content for Na_xSi₁₃₆. The room temperature transport data is from Figure 12.

Synthesis and structural characterization of single-crystal K_{7.5}Si₄₆ and K_{17.8}Si₁₃₆ clathrates We can employ KCTD for the selective synthesis of other clathrates, such as K_{7.5}Si₄₆ and K_{17.8}Si₁₃₆ single-crystals.[47] The potassium containing clathrate-II silicon is synthesized unequivocally for the first time, reflecting substantial promise of this approach to obtain novel clathrate-II compositions, of which only a handful are known outside of the work conducted under this project.[1, 46] K₄Si₄ precursor was synthesized by direct reaction of elemental K (Alfa Aesar, 99.98%) and Si (Alfa Aesar, 99%) powder in a K:Si atomic ratio of 1.1:1. The reaction was carried out inside a tungsten crucible that was inside a sealed stainless steel canister at 550 °C for 36 hours. The resulting product was a dark gray crystalline material which was then coarsely ground into powder in a dry nitrogen atmosphere. By maintaining a sufficient partial pressure of the alkali metal over graphite, K was removed from the K₄Si₄ precursor resulting in single-crystal formation. The crystals were synthesized by maintaining the precursor at 550 °C and 625 °C for the clathrate-I and II compositions, respectively, for 15 hours (Figure 14). No change in the precursor was observed at temperatures below 500 °C. Annealing the precursor at temperatures higher than 650 °C and longer than 24 hours lead to the formation of the α-Si phase. The product of the reaction was separated from the unreacted K₄Si₄ by washing with ethanol and distilled water. The K_{7.5}Si₄₆ crystals formed in relatively uniform cubes 100 – 200 μm in length whereas the K_{17.8}Si₁₃₆ crystals form in a pyramidal habit < 100 µm on the longest side. Structural analyses were performed using single-crystal X-ray diffraction. The Ueq values indicated no "rattling" for K@Si20 in K7.5Si46, similar to Na@Si20 in Na8Si46. This is in contrast with K@Si28 in K17.8Si136, where "rattling" was

observed, however not as pronounced as for Na@Si₂₈ in Na₂₄Si₁₃₆.[47] This research also allowed for an investigation of the intrinsic transport properties of these materials.[47]

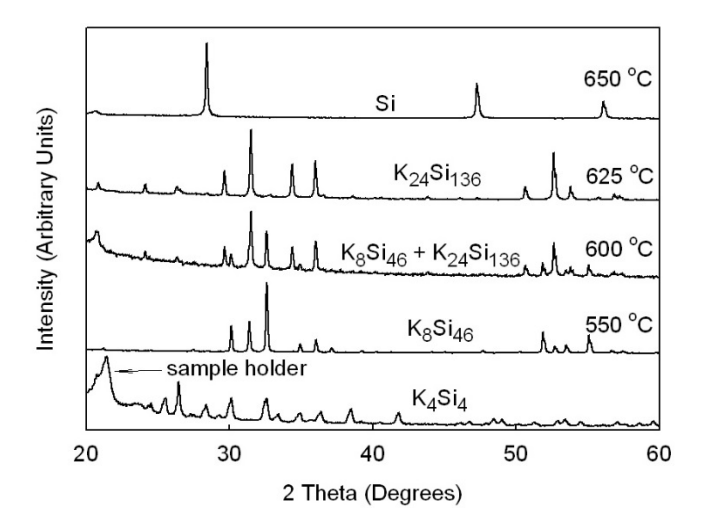


Figure 14. Formation of different phases at different temperatures starting from the same precursor K₄Si₄. The single-crystal products were crushed in order to perform powder XRD.

Spark plasma sintering: Cystal growth optimization

The crystallinity of clathrate-I Na₈Si₄₆ and clathrate-II Na₂₄Si₁₃₆ was also investigated as a function of applied pressure and temperature employing SPS.[48] Specimens with the clathrate-I and II crystal structures were synthesized by SPS processing of Na₄Si₄ at the respective temperatures of 450 °C and 600 °C, and uniaxial pressures of 60, 80, and 100 MPa for 3 hours. I note that this investigation also revealed the optimum SPS parameters for the selective synthesis of these clathrate compositions. The temperature ramp rates were 100 °C /min for the clathrate-I phase, and 25 °C /min up to 450 °C and then 10 °C /min up to 600 °C for the clathrate-II phase. Selective synthesis was achieved by choosing the appropriate temperature, 450 °C for the clathrate-I phase and 600 °C for the clathrate-II phase. No change in the precursor was observed at temperatures below 400 °C. At 550 °C a mixture of both phases was observed. SPS processing at 650 °C yields the α-Si phase. The highest yield of single crystals was achieved at 450 °C and 600 °C for the clathrate-I and II phases, respectively, at 100 MPa. This approach allowed for the selectivesynthesis of single-crystal and microcrystalline Na₈Si₄₆ and Na₂₄Si₁₃₆ as a function of the applied pressure. At 60 MPa high purity microcrystalline products were observed. When the pressure was increased from 60 MPa to 80 MPa, clathrate-II single crystals started to form but clathrate-I single crystals formed at 100 MPa. The average size of the single crystals was obtained from SEM analyses. The average size of the clathrate-I phase does not change as the pressure is increased from 60 to 80 MPa, in contrast to the clathrate-II phase. The average crystal size for the clathrate-II phase at 80 MPa is smaller than that at 100 MPa, suggesting that the crystal size increases with increasing pressure. Table I contains these SPS processing conditions and resulting materials and morphologies.

SPS processing at 60 and 80 MPa resulted in only microcrystalline Na₈Si₄₆, whereas at 100 MPa only single crystals were observed at the appropriate temperatures. The average size of the single-crystal products, 150 μ m and 250 μ m for the clathrate-I and II phase, respectively, is comparable to that obtained by our other single-crystal synthesis method. At 550 °C and 100 MPa a mixture

of powders and single crystals of both clathrate phases was observed. The relative clathrate fraction in the synthesis product as a function of reaction time was also investigated. When the precursor was reacted at 600 °C for 30 minutes, the clathrate-I phase was estimated to be approximately 60 % whereas the clathrate-II phase was approximately 40%, from powder XRD analyses. As the reaction time increased at the same temperature, the intensity of the clathrate-I reflections in the XRD spectra decreased. For a reaction time of 3 hours only the clathrate-II phase was observed. The average size of Si obtained by SPS processing of the Na₄Si₄ precursor at 650 °C was 65 nm; therefore this approach can also yield nano-sized Si. The high heating rates and localized heating in the SPS, considered two of the most important factors for the synthesis of Si nanoparticles, may be an indication that SPS is also a promising method for the synthesis of Si nanoparticles.

Table I. Processing conditions for SPS synthesis from the precursor Na₄Si₄.

T (°C)	P (MPa)	Phase	Crystallinity	L (µm)
450	60	clathrate-I	microcrystalline	10
	80	clathrate-I	microcrystalline	10
	100	clathrate-I	single crystal	150
550	60	clathrate-I+II	microcrystalline	10
	80	clathrate-I+II	microcrystalline + single crystal	10/150
	100	clathrate-I+II	microcrystalline + single crystal	10/150
600	60	clathrate-II	microcrystalline	15
	80	clathrate-II	single crystal	50
	100	clathrate-II	single crystal	250
650	100	Silicon	nano-crystalline	0.065

SPS can also be successfully employed for the synthesis of the type-I a Si-Ge alloy clathrates. SPS processing of a Na₄(Si₄Ge)₄ precursor with a 50/50 Si/Ge molar ratio at 450 °C for one hour resulted in the synthesis of Na₈Ge_{2.8}Si₄₀. The lattice parameter, 10.2133(21) Å, for this composition is slightly larger than that of Na₈Si₄₆. The refined atomic coordinates and U_{eq} values for Na1 and Na2 are much larger than that of the framework atoms, which may be an indication of dynamic disorder of Na inside the polyhedral cavities. U_{eq} for Na2 are relatively large, however they are smaller than those of Na1. Even though Na2 is encapsulated within the larger polyhedron, it exhibits lower U_{eq} as compared to that of Na1. This is due to the vacancies present on the 6ccrystallographic sites that presumably result in shrinkage of the size of the larger polyhedra, therefore reducing the available "room" for Na2 to "rattle". The interstitial 2a and 6d crystallographic sites are fully occupied with Na, and the framework 16i and 24k are fully occupied with Si. The 6c site is partially occupied by Si and Ge. In addition, the Na2 atoms that are typically found to exhibit anisotropic atomic displacement parameters due to the lower symmetry of the larger polyhedral cavities, are now found to be isotropic. This is presumably related to the presence of vacancies at the 6c crystallographic sites which result in distortion of the larger polyhedra. The 6c crystallographic sites are associated with the atoms residing on the hexagonal rings of the larger tetrakaidecahedra. Therefore, the presence of vacancies at the 6c crystallographic site results in an increase of the symmetry of these tetrakaidecahedra, and therefore isotropic ADPs for the Na atoms encapsulated in their polyhedral cavities. The atomic distances for Na₈Ge_{2.8}Si₄₀, obtained from our refinement results, indicate that the Si-Si distances are comparable to those of the Na₈Si₄₆ and K_{7.5}Si₄₆ clathrates, whereas the Si-Ge distances are slightly larger than the Si-Si distances presumably due to the larger radius of Ge as compared to Si. This also results in a larger lattice parameter for Na₈Ge_{2.8}Si₄₀ as compared to that of the type I clathrates Na₈Si₄₆ and K_{7.5}Si₄₆. The larger lattice parameter of Na₈Ge_{2.8}Si₄₀ is consistent with the larger Na-Ge distances as compared to the Na-Si distances.

Ionic liquid synthesis

The synthesis of Na₈Si₄₆ and Na₂₄Si₁₃₆ without clathrate impurity phases and in relatively high yield was achieved by oxidation of Na₄Si₄ from the byproduct of the decomposition of the ionic liquid (IL) ndodecyltrimethylammonium chloride (DTAC) combined with AlCl₃.[49] Unlike previous studies [50, 51] we separate the IL from the precursor in order to avoid secondary clathrate or amorphous phases.[52] The thermal decomposition of the IL supplied the oxidizing agent, mainly HCl.[53] The HCl is further reduced to H₂ as the chloride reacts with the akali metal anions, forming a stable byproduct, such as NaCl as observed in this study. Maintaining separation of the IL from the precursor together with careful control of the synthetic parameters, temperature and time in particular, allowed for the synthesis of both clathrate structure types without need for further annealing. When the precursor Na₄Si₄ was reacted for a period of 24 hours at temperatures of 210 to 240 °C, the result was the type II clathrate Na₂₄Si₁₃₆. Reactions at similar temperatures for 8 hours result in type I clathrate Na₈Si₄₆ formation. The highest yield of Na₂₄Si₁₃₆, 20 % by weight with only α-Si as the impurity phase, was synthesized by reacting at 210 °C for 24 hours. I note that α-Si was always observed in the synthesis of microcrystalline Na₂₄Si₁₃₆, and is one of the main reasons that we have developed two new and unique crystal-growth and processing techniques under this project, KCTD and SPS. Nevertheless, phase pure type I clathrate Na₈Si₄₆ was obtained with a similar yield at 240 °C and a reaction time of 8 hours.

Microcrystalline and single crystal Na₈Al₈Si₃₈ synthesized for the first time

A mixture of Na₄Si₄ and Na₄Si₅ was used as the precursor for SPS and KCTD synthesis of Na₈Al₈Si₃₈.[54] This composition is of particular interest for potential thermoelectric applications, and has until now not been successfully synthesized. Single crystals of Na₈Al₈Si₃₈ were grown by the KCTD technique, while microcrystalline powders were synthesized by SPS processing (Figure 15). Reaction of Na₄Si₄ and NaAlSi with a mole ratio of 7.5:8 at 690°C for 9 hours yielded Na₈Al₈Si₃₈. Our refinement results indicated a lattice parameter of 10.3241(7)Å, larger than that of Na₈Si₄₆ (10.1962(9)Å) as expected due to the larger atomic size of Al (r = 1.43 Å) as compared with Si (r = 1.17Å). This reaction process can be thought of as the equilibrium reaction 7.5Na₄Si₄ + 8NaAlSi \rightarrow Na8Al8Si38 + 30Na. The Na vapor phase is gradually absorbed by the graphite layer, therefore the reaction constantly advances toward the synthesis of Na₈Al₈Si₃₈. This approach allows for the slow release of Na in the vapor phase which then allows for the reaction to take place at higher temperatures providing adequate energy for the formation of Na₈Al₈Si₃₈. This may explain why the synthesis of Na₈Al₈Si₃₈ has not been previously reported, although attempted often by different synthetic techniques including high pressure techniques. Using a molar ratio of 7.5Na₄Si₄ to 8NaAlSi, Na₈Al₈Si₃₈ was synthesized at any temperature between 620 to 720 °C. This represents a much wider temperature range compared to Na₈Si₄₆ (pure phase Na₈Si₄₆ forms between 580 and 590 °C). On the other hand pure Na₈Al₈Si₃₈ can be obtained even when the annealing time is prolonged to 48h. These results indicate the high thermal stability of Na₈Al₈Si₃₈.

Single crystals of Na₈Al₈Si₃₈ were grown by the KCTD technique. The precursor, a NaAlSi / NaSi mixture, was placed in custom designed stainless steel tooling under a uniaxial pressure of 20 MPa and heated at 953 K for 9h under a dynamic vacuum of 10⁻⁶ Torr and phase pure Na₈Al₈Si₃₈ in the form of single-crystals was obtained. The UV/Vis diffuse reflectance spectrum (Figure 16) indicats an optical band gap of 0.64 eV, similar to that of the theoretical indirect gap of the hypothetical guest free Si₄₆ (0.7 eV) and α-Ge (0.74 eV). The band gap originates mainly from transitions involving filled 3s and 3p of Al and Si hybridizations in the valence band and empty Al and Si 3s and 3p hybridizations in the conduction band. The contributions from Na ions near the Fermi levels can be expected to be minimal due to their strong ionic bonding character with the Al₈Si₃₈ framework. Consequently, the band gap is determined by the Al₈Si₃₈ framework. This is presumably why the band gap of Na₈Al₈Si₃₈ is similar to that reported for K₈Al₈Si₃₈ using density functional calculations.[55]

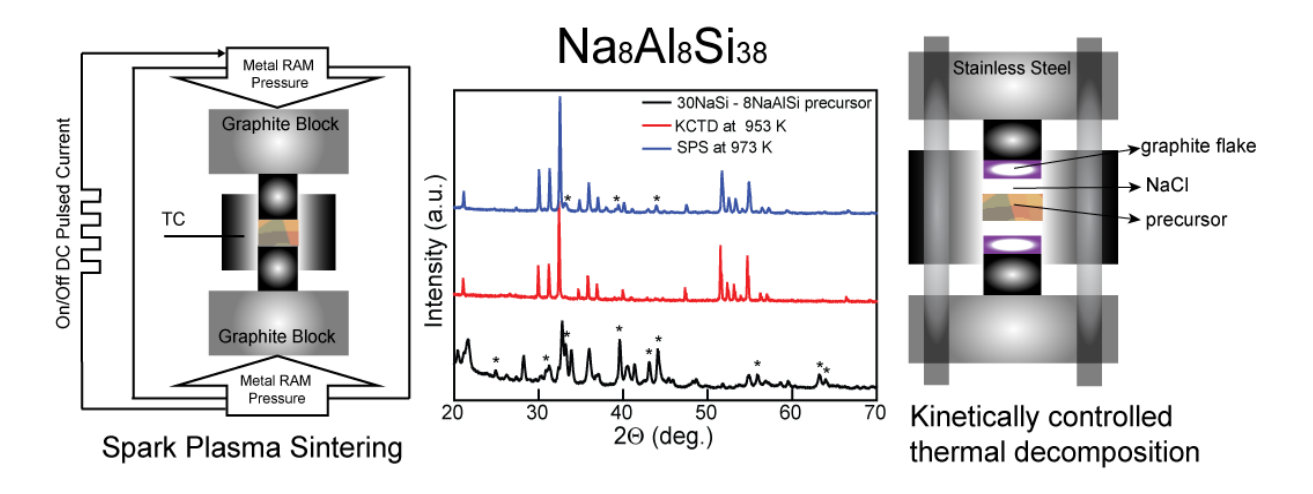


Figure 15. The novel synthetic techniques developed under this DOE project have been employed in processing new multinary clathrate compositions that have until now not been obtained, and therefore also allowed for the investigation of their physical properties for the first time. Both SPS and KCTD have been employed in the synthesis of the ternary intermetallic clathrate Na₈Al₈Si₃₈ using a mixture of Na₄Si₄ and NaAlSi as the precursor.[54]

As shown in Figure 17, the electrical conductivity, σ , and modulus of S values increase with increasing temperature. The negative S values throughout the entire measured temperature range, 300 to 500 K, implies electron conduction. The increase in σ with temperature was very small, as is typical for thermally activated semiconductor behavior. The room temperature S value (-22 μ V/K) was smaller than that of A₈Al₈Si₃₈ (A = K, Rb, Cs) and comparable to that of other Al containing clathrate-I compounds such as Ba₈Al₁₄Si₃₁ (-21 μ V/K) and Ba₈Al₁₆Si₃₀ (-48 μ V/K).[54] The measured κ decreases with increasing temperature, typical of dielectric behavior. The room temperature κ value (2.0 W/mK) was slightly larger than that of A₈Al₈Si₃₈ (A = K, Rb, Cs) presumably due to the higher σ value, but much smaller than Na₈Si₄₆.

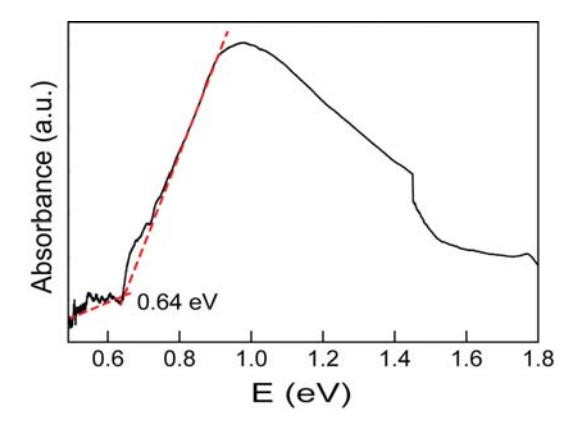


Figure 16. Solid-state UV / Vis absorption spectra of Na₈Al₈Si₃₈. A value of 0.64 eV is obtained from the intersection of the fitted base line and absorption edge (red dotted line).

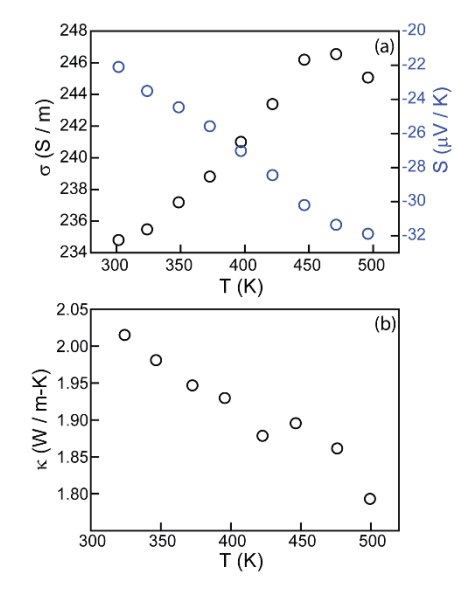


Figure 17. Temperature-dependent (a) σ (black circles) and S (blue circles), and (b) κ for Na₈Al₈Si₃₈.

The refined unit cell parameters and bond distances of Na₈Al₈Si₃₈ are larger than those of Na₈Si₄₆ (a = 10.1962(9) Å) [36] due to the inclusion of Al on the framework, but smaller than those of A₈Al₈Si₃₈ (A = K, Rb, Cs) [55, 56] and Ba₈Al₈Si₃₈ [57] due to the smaller ionic size of the encapsulating Na atoms. Indeed, a plot of the lattice parameter versus ionic radii (coordination number CN = 12) [58] for A₈Al₈Si₃₈ (A = Na, K, Rb, Cs, and Ba) is relatively well described by a linear relationship (Figure 18).

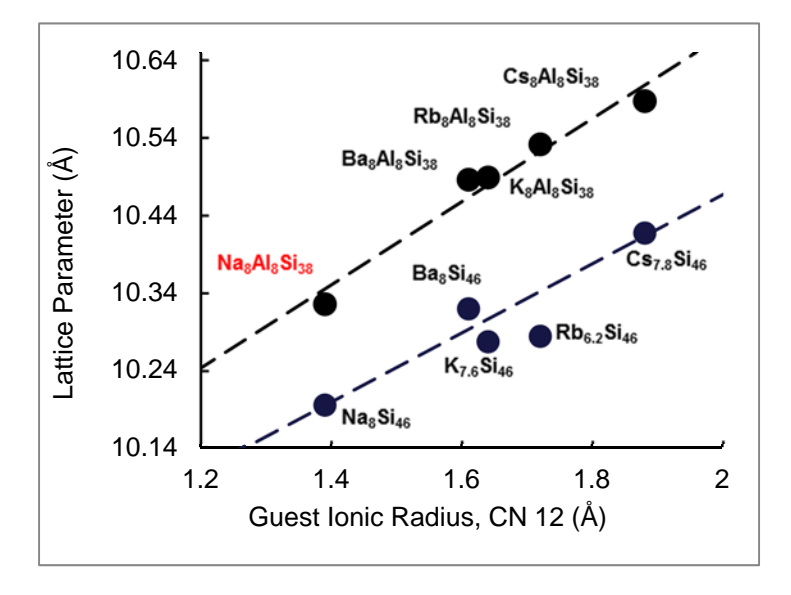


Figure 18. A plot of the lattice parameters versus ionic radii (coordination number CN = 12) of the guest atoms for $A_8Al_8Si_{38}$ (A = Na, K, Rb, Cs, and Ba) and A_8Si_{46} .

Synthesis and structural characterization of Si-Ge alloy clathrates

A Na₄(Si_{0.9}Ge_{0.1})₄ precursor was used to synthesize single crystal type-II Na₂₄(Si_{0.9}Ge_{0.1})₁₃₆ by KCTD for the first time. Large single crystals of nominal composition Na₂₄(Si_{0.9}Ge_{0.1})₁₃₆ were successfully grown at 665 °C for 9 hours. As is the case for Na₂₄Si₁₃₆, the Na₂₄(Si_{0.9}Ge_{0.1})₁₃₆ single crystals form in polyhedral shapes, the largest being approximately 0.2×0.2×0.2 mm³ in size. The Na₂₄(Si_{0.9}Ge_{0.1})₁₃₆ phase can also be synthesized at lower temperatures, however the crystal size decrease with decreasing reaction temperature. Energy dispersive X-ray spectroscopic (EDX) analysis was used to investigate the single crystals and consistently indicated that Ge was present in the crystals.

Both traditional thermal decomposition and KCTD were employed for Si-Ge alloy clathrate synthesis with $K_4(Si_{1-x}Ge_x)_4$ as precursors.[59] $K_4(Si_{1-x}Ge_x)_4$ alloys were synthesized by reacting elemental potassium and ball milled $Si_{1-x}Ge_x$ alloys, in a 1.4: 1 molar ratio, at 668 K for 24 h under flowing Ar. The precursor synthesis technique employed in this work was relatively simple and achieved without need of sealed crucibles. $K_4(Si_{1-x}Ge_x)_4$ with x = 0.1, 0.3, and 0.75 were heated to 823 K for 8h, 803 K for 8h, and 758 K for 5h, respectively, to obtain type-I alloy clathrates. The final clathrate compounds were stable in air. The phase purity and crystal structure of the specimens were determined by XRD at room temperature. The Si-to-Ge ratios of the clathrate phases were closer to that of the precursors and the site occupancy for the Si/Ge framework followed the same trend as that exhibited by the clathrates prepared by thermal decomposition. The highest Ge content clathrate, $K_{7.6}Si_{14.9}Ge_{31.1}$, contained amorphous Ge. The lattice constants obeyed Vegard's law, exhibiting a linear increase with increasing germanium content. The two compounds with vacancies on the 2a site deviated only slightly from Vegard's law.

The phase purity and crystal structure of the specimens were determined by powder X-ray diffraction (XRD) at room temperature. The Si-to-Ge ratios of the clathrate phases are closer to that of the precursors and the site occupancy for the Si/Ge framework follows the same trend as that exhibited by the clathrates prepared by thermal decomposition. The highest Ge content clathrate, K_{7.6}Si_{14.9}Ge_{31.1}, contained amorphous Ge. The lattice constants with Ge concentration for all clathrates compounds are shown in Figure 19 and obey Vegard's law, exhibiting a linear increase with increasing germanium content. The two compounds with vacancies on the 2a site deviate only slightly from Vegard's law. [59]

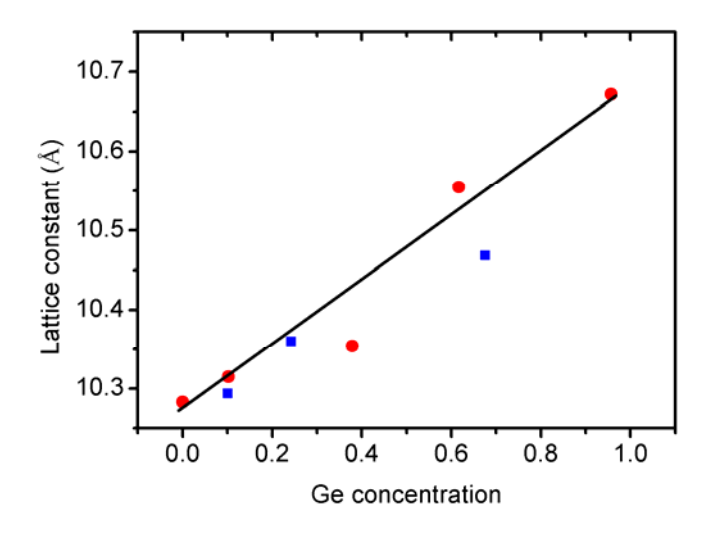


Figure 19. Lattice constant as a function of Ge concentration for the clathrates prepared by thermal decomposition (red) and KCTD (blue).

Investigations of new synthetic route for the preparation of clathrate-II compositions

As described above, an electrochemical redox reaction initiated by the applied electric current that passes through the specimen during SPS processing induces crystal growth, with the Na₄Si₄ precursor acting like a solid electrolyte with sodium transport toward the cathode. We also demonstrated that the selective synthesis of binary Na-Si clathrate-I and -II compositions was possible by changing the applied SPS conditions. It is well known that pure alkali metals such as K, Rb, and Cs can be obtained by ion-exchange employing their chlorides (ACl with A = K, Rb, Cs) with Na at high temperatures. We hypothesized that combining these two approaches will lead to a simultaneous electrochemical redox reaction together with an ion-exchange reaction. When combining Na₄Si₄ together with ACl, the tetrahedral Si₄⁴⁻ units from the Na₄Si₄ precursor start to oxidize to form the clathrate framework at the anode while elemental Na is formed by reduction of the Na⁺ ions at the cathode. During this process Na also reacts with ACl to form NaCl allowing A to be available for encapsulation in the resulting polyhedra of the clathrate framework. Using this knowledge, we also successfully synthesized three clathrate–II compositions (A8Na₁₆Si₁₃₆), as shown in Figure 20, investigated the synthesis of new compositions employing this approach, and selectively synthesized ternary clathrate-I and II compositions with SPS processing temperature.[60]

Single crystals of three type-II clathrates, $K_{5.8(1)}Na_{16}Si_{136}$, $Rb_8Na_{16}Si_{136}$, and $Cs_8Na_{16}Si_{136}$, were synthesized by SPS for the first time.[60] The NaSi precursor along with each alkali-metal chloride were ground together in a 1:1 mass ratio. Pulsed DC current was sourced through the precursor mixture and die assembly while under a uniaxial pressure of 100 MPa in a vacuum of 10 mTorr. The dwell time at the desired temperature (873 K for $K_{5.8(1)}Na_{16}Si_{136}$, 838 K $Rb_8Na_{16}Si_{136}$, and 773 K for $Cs_8Na_{16}Si_{136}$) for each reaction was 1.5 hr. The product of each reaction was separated from any unreacted NaSi and ACl by washing with ethanol and distilled water. The U_{eq} values of Rb in $Rb_8Na_{16}Si_{136}$ and $Cs_8Na_{16}Si_{136}$ are relatively small with $U_{eq} = 0.0296$ Å² and $U_{eq} = 0.0168$ Å², respectively, and very similar to those previously reported. The potassium atoms in $K_{5.8(1)}Na_{16}Si_{136}$ have room temperature atomic displacement parameter values that are 2 to 3 times larger ($U_{eq} = 0.0695$ Å²) implying that the K atoms partially occupy the Si_{28} polyhedra while possessing a more dynamic disorder inside the Si_{28} polyhedra, as compared with that of Rb and Cs in the other clathrates, due to its relatively smaller ionic size.

Crystal growth by SPS is influenced by the pulsed DC current; however, in the present case an electrochemical redox reaction occurs simultaneously with an ion-exchange reaction. Considering that the reaction occurs completely, we postulate that the reaction process is as follows: 136 NaSi + 8 ACl \rightarrow A₈Na₁₆Si₁₃₆ + 8 NaCl + 112 Na. Here tetrahedral Si₄⁴ units from the NaSi precursor start to oxidize to form Si₁₃₆²⁴⁻ at the anode while elemental Na is formed by reduction of Na⁺ ions at the cathode through an electrochemical redox reaction. During this process Na⁺ ions also react with ACl to form NaCl allowing K, Rb or Cs, together with the remaining Na atoms, to be available for encapsulation in the resulting polyhedra of the clathrate framework. Our results also indicated that reaction time does not substantially affect the yield or size of the single crystals. This approach can also be employed for the synthesis of other compositions; the polycrystalline ternary silicide compound Li₃NaSi₆ was synthesized by this approach when using LiCl and NaSi mixtures as the precursor.

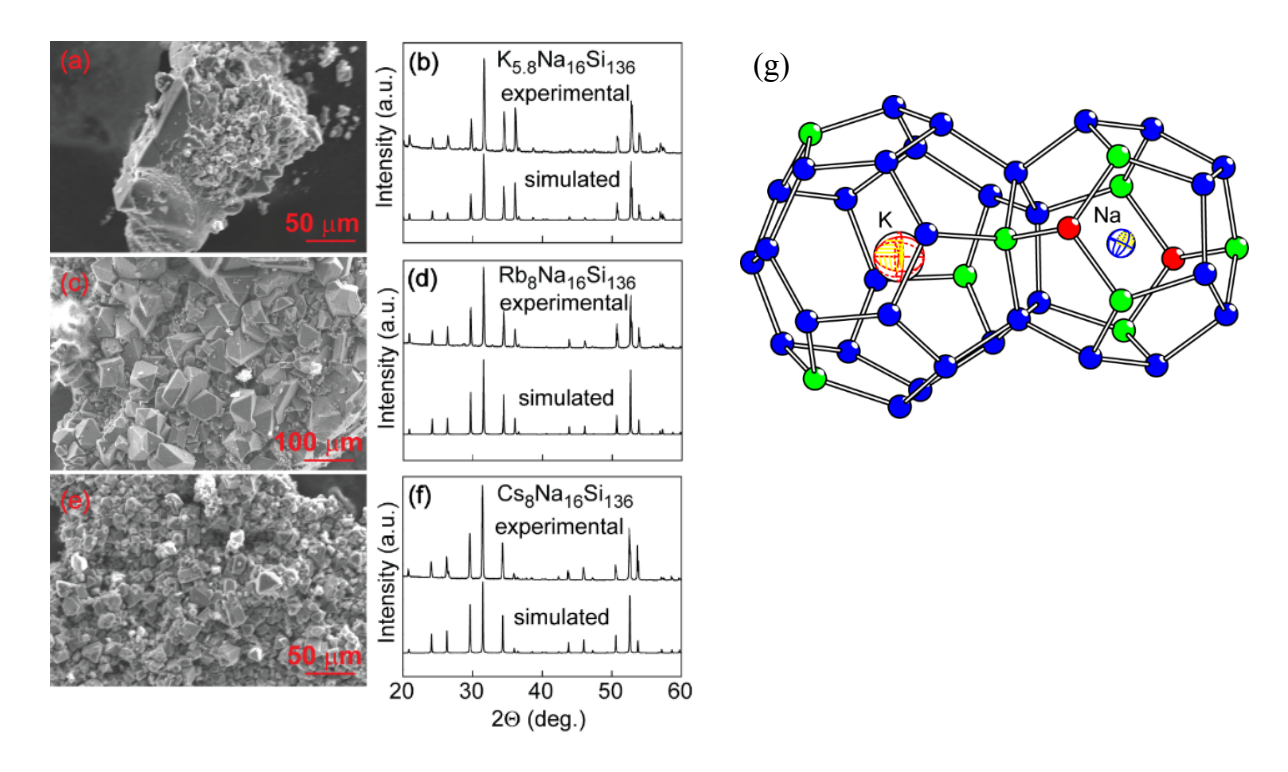


Figure 20. SEM images of the clathrate single crystals and powder XRD patterns from crushed single crystals for (a) and (b) K_{5.8(1)}Na₁₆Si₁₃₆, (c) and (d) Rb₈Na₁₆Si₁₃₆, and (e) and (f) Cs₈Na₁₆Si₁₃₆, along with their simulated powder pattens. (g) Hexakaidekahedron (Si₂₈) and dodecahedron (Si₂₀) with corresponding alkali metal atoms in K_{5.8(1)}Na₁₆Si₁₃₆. Thermal ellipsoids for K (8*b*) and Na (16*c*) are 90 % probability. Blue, green, and red atoms indicate Si on the 96*g*, 32*e*, and 8*a* crystallographic sites, respectively.

Clathrate-II Cs8Na₁₆Al₂₄Si₁₁₂ synthesized and low temperature transport

We synthesized a quaternary intermetallic silicon clathrate-II compound by KCTD by employing a precursor that was a mixture of NaSi and NaAlSi together with the alkali metal halide CsCl, in effect, a multiprecursor ion exchange synthetic approach (Figure 21).[61] This is the first time a clathrate-II Al-Si framework composition was reported. Structural refinement indicates full occupancy of the framework and that Cs and Na reside at the crystallographic 8b and 16c sites, respectively. The framework bond distances, as well as powder XRD refinement and elemental analysis, indicate that Al atoms were present on the framework sites. Transport properties, investigated from 12 to 300K, and solid state UV-Vis diffuse reflectance measurements show semimetallic behavior with electron conduction. The modulus of S increases linearly with increasing temperature throughout the measured temperature range while the ρ values increase with increasing temperature above 75 K. The measured room temperature $S(-32 \mu V/K)$ is smaller than that of $A_8A_18S_{138}$ (A = K, Rb, Cs) but comparable to that of other Al containing clathrate-I compounds such as Na₈Al₈Si₃₈ (-22 μ V/K), Ba₈Al₁₄Si₃₁ (-21 μ V/K) and Ba₈Al₁₆Si₃₀ (-48 μV/K).[61] Although our refinement and EDS results do not allow us to quantify the aluminum content precisely, our electrical transport data suggest that the Al content is less than the target Cs₈Na₁₆Al₂₄Si₁₁₂ content. Semiconducting behavior is expected for Cs₈Na₁₆Al₂₄Si₁₁₂, from simple

crystal chemistry arguments, however deviation from this stoichiometry will result in a metallic S and ρ temperature dependence. The measured κ values increase up to 200 K after which point they decrease with increasing temperature. This behavior is similar to that of Cs₈Na₁₆Ge₁₃₆ and Na₂₄Si₁₃₆, although our κ values are much smaller than that of these two compositions. Our results indicate that the KCTD synthetic method can be employed for the synthesis of multinary inorganic clathrate phases that cannot be accessible by traditional crystal growth techniques.

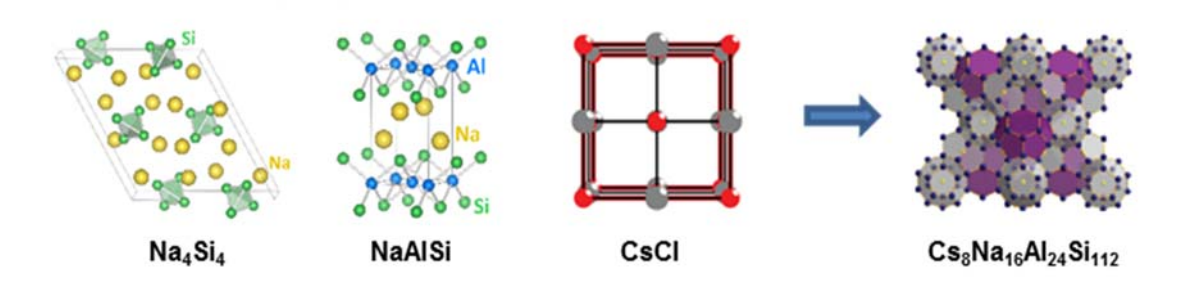


Figure 21. Schematic illustration of the multi-precursor, ion-exchange approach for processing quaternary clathate-II compositions employing KCTD.

Clathrate-II (K,Ba)16(Ga,Sn)136 synthesized and densified employing SPS

Tin clathrate-II framework-substituted compositions are of current interest as potential thermoelectric materials for medium-temperature applications. Potassium and barium filled, gallium framework substituted tin clathrate-II single crystals were synthesized in large quantities so that they may be ground to fine powder for densification employing optimized SPS parameters to form dense bulk polycrystalline specimens for high temperature transport properties measurements.[62] To prepare the specimens, the elements with an excess of Ga and Sn relative to the appropriate stoichiometric rations were loaded into a tungsten crucible that was then sealed inside a custom-designed stainless steel vessel, with all synthetic procedures occurring inside a nitrogen glovebox. The stainless steel vessel was then transferred into a glass tube and sealed under vacuum. The glass tube was put into a furnace at 923 K for 15 h, followed by slow cooling to 723 K at a rate of one degree per minute before being air cooled to room temperature. The products of this reaction included clathrate-II (K,Ba)₁₆(Ga,Sn)₁₃₆, clathrate-I (K,Ba)₈(Ga,Sn)₄₆, BaSn₃, Ba₂Sn₃, Ba₂Sn, as well as elemental Sn and Ga. A mixture of 10 mL HCl, 10 mL HNO₃, and 80 mL DI water was used to remove this remaining flux from the resulting products, thus allowing for easy separation of the clathrate-II crystals from the other phases.

Our PXRD refinement results indicated a mixed occupancy in the $(Ga,Sn)_{20}$ dodecahedra, vacant $(Ga,Sn)_{28}$ hexakaidecahedra, and no vacancy on the framework. This type of preferential polyhedral occupancy can be related to the relative sizes of the constituent atoms. Transport properties of the specimens were investigated from 12 to 300K.[62] The temperature-dependent S data indicates possible bipolar diffusion. The ρ trends somewhat with composition, $K_{2.9(4)}Ba_{13.1(2)}Ga_{23.2(3)}Sn_{112.7(5)}$ possessing lower ρ values in the measured temperature range as compared with $K_{7.1(2)}Ba_{8.8(3)}Ga_{25.1(4)}Sn_{110.8(3)}$, which showed more semiconducting-like behavior. This is expected, given the simple chemical analysis whereby each Ga acts as an acceptor for each

donated electron from K⁺ and Ba²⁺. Room temperature Hall measurements indicated carrier concentrations of 3.1×10^{19} cm⁻³ and 6.2×10^{19} cm⁻³ for K_{7.1(2)}Ba_{8.8(3)}Ga_{25.1(4)}Sn_{110.8(3)} and K_{2.9(4)}Ba_{13.1(2)}Ga_{23.2(3)}Sn_{112.7(5)}, respectively, values that are in the same order-of-magnitude as that of previous reports on clathrate-II Sn compositions. From our measured room temperature carrier concentration and *S* values, and assuming a simple parabolic band model, we estimated effective mass, m^* , of the two specimens to be $0.45m_e$ and $0.51m_e$ for K_{7.1(2)}Ba_{8.8(3)}Ga_{25.1(4)}Sn_{110.8(3)} and K_{2.9(4)}Ba_{13.1(2)}Ga_{23.2(3)}Sn_{112.7(5)}, respectively. A plateau in the *ZT* values at higher temperatures was observed for both specimens, with the highest *ZT* value (0.6) achieved for K_{2.9(4)}Ba_{13.1(2)}Ga_{23.2(3)}Sn_{112.7(5)} at 575 K.

Type-II clathrate with a Li-Ge framework synthesized and characterized for the first time The first intermetallic type-II clathrate phase with Li-substituted framework Na₁₆Cs₈Li_xGe_{136-x} was obtained with composition $x \approx 2.8$ by reaction of the elements at 650 °C.[63] The phase composition was established from crystal structure refinement supported by NMR spectroscopy, microstructure and chemical analyses. In the type-II clathrate crystal structure (space group Fd 3m), Li atoms substitute Ge atoms at site 96g. This may be rationalized by the Zintl concept with the formation of tetrahedral [LiGe₄]³⁻ units constituting 3-electron acceptors that compensate a part of the excess electrons from Na and Cs and provide a favorable coordination environment for Li atoms. Due to the somewhat shorter Li-Ge bonding distance compared to Ge-Ge, the lattice parameter of the new quaternary phase is smaller by about 0.2 % than that of the ternary prototype Cs₈Na₁₆Ge₁₃₆ clathrate. From the observed NMR Knight shifts for ⁷Li, 23Na and ¹³³Cs it is evident that $Cs_8Na_{16}Li_xGe_{136-x}$ (x \approx 2.8) is metallic. Comparison of NMR results and magnetic susceptibility with the ternary Cs8Na₁₆Ge₁₃₆ clathrate and literature data suggest that there is specific electronic interaction of Cs with the [LiGe₄]³⁻ framework entities. Although a number of details on the homogeneity range and interatomic interaction, and their impact on the physical properties, are as yet to be investigated, the successful preparation of Cs₈Na₁₆Li_xGe_{136-x} is a unique framework substitution by Li in clathrate-II compositions. As effectively a 3-electron acceptors, framework-substitution by Li atoms provides a versatile and inexpensive alternative to the (quasi) isoelectronic metals for the preparation of charge-compensated semiconducting intermetallic clathrates that are of potential interest for a variety of technological applications.

Bulk polycrystalline materials with nano-scale grains via SPS

Systems with reduced dimensions have shown superior thermoelectric performance. However, utilizing such materials for practical applications may be challenging. The manufacture of thermoelectric devices requires materials in large quantities, a key reason why device-level development is currently difficult to achieve for superlattice and nanowire materials. Therefore, the dimensional integration of bulk thermoelectric materials with nanoscale features resulting in ZT ($=S^2/\rho\kappa$) enhancement has been in the spotlight as a viable route for increasing ZT. By employing SPS our group has demonstrated that carefully engineered nanostructured materials can result in enhanced thermoelectric performance as compared to their bulk counterparts. Moreover, nano-structured bulk polycrystalline compositions, particularly materials that have relatively low decompositions temperatures, were prepared through bottom-up processing and densified using SPS in order to investigate their transport and thermoelectric properties. [64-67] For all the specimens that have been investigated, κ was greatly reduced due to smaller average grain size and therefore significant grain-boundary phonon scattering. These results demonstrate that bottom-up synthesis followed by optimized SPS processing can result in dense polycrystalline thermoelectric

materials, and is a powerful approach for physical properties investigations of materials with nanoscale grains or inclusions.

Conclusions

One key aspect of this research was the development of new synthetic approaches that allow for an investigation of novel clathrate materials for the first time. Typically, new materials or compositions of scientific or technological importance cannot be synthesized by well-known or established approaches. For such materials new synthetic approaches are required. This work establishes new approaches demonstrating that field-assisted (employing spark plasma sintering, SPS) and kinetically controlled thermal decomposition (KCTD) techniques can be employed for the synthesis of compounds that otherwise cannot be synthesized. These new techniques added to the more established crystal growth and microcrystalline synthetic approaches allowed for the investigation of the physical properties of a variety of new clathrate compositions and structure types. A wide range of physical properties measurements were employed in order to fully characterize the structure, chemical, electrical and thermal properties of the materials developed, synthesized and investigated in this research project. The techniques described in this report can be employed for the synthesis and crystal growth of other intermetallic or metastable compounds. It is clear that these results will greatly aid the scientific community in expanding the knowledgebase of potential clathrate compositions, and potentially further the advance of these materials for technological applications.

References

- 1. Book. G.S. Nolas, editor, The Physics and Chemistry of Inorganic Clathrates, Springer, 2014.
- 2. C. Cros, M. Pouchard and P. Hagenmuller, J. Solid State Chem. 2, 570 (1970).
- 3. M. Beekman, E.N. Nenghabi, K. Biswas, C.W. Myles, M. Baitinger, Y. Grin and G.S. Nolas, Inorg. Chem. **49**, 5338 (2010).
- 4. M. Beekman, W. Wong-Ng, J.A. Kaduk, A. Shapiro and G.S. Nolas, J. Solid State Chem. 180, 1086 (2007).
- 5. M. Beekman, J.A. Kaduk, J. Gryko, W. Wong-Ng, A. Shapiro and G.S. Nolas, J. Alloys Comp. **470**, 365 (2009).
- 6. K. Biswas and C.W. Myles, Phys. Rev. B 74, 115113 (2006).
- 7. R.N. Hall and J.H. Racette, J. Appl. Phys. 35, 379 (1964).
- 8. K. Biswas and C.W. Myles, Phys. Rev. B 75, 245205 (2007).
- 9. M. Beekman, J.A. Kaduk, Q. Huang, W. Wong-Ng, W. Yang, D. Wang and G.S. Nolas, Chem. Commun. **837** (2007).
- 10. M. Beekman, S. Stefanoski, W. Wong-Ng, J.A. Kaduk, Q. Huang, C. Reeg, C.R. Bowers and G.S. Nolas, J. Solid State Chem. **183**, 1272 (2010).
- 11. S. Stefanoski, G. Finkelstein, M. Ward, T. Zeng, K. Wei, E. Bullock, C. Beavers, H. Liu, G. Nolas and T. Strobel, Chem. Mater., submitted, 2017.
- 12. M. Beekman, M. Baitinger, H. Borrmann, W. Schnelle, K. Meier, G.S. Nolas and Yu. Grin, J. Am. Chem. Soc. **131**, 9642 (2009).
- 13. G.K. Ramachandran, J.J. Dong, J. Diefenbacher, J. Gryko, R.F. Marzke, O.F. Sankey and P.F. McMillan, J. Solid State Chem. **145**, 716 (1999).
- 14. E. Reny, P. Gravereau, C. Cros and M. Pouchard, J. Mater. Chem. 8, 2839 (1998).

- 15. H. Horie, T. Kikudome, K. Tramura and S. Yamanaka, J. Solid State Chem. 182, 129 (2009).
- 16. M. Beekman and G.S. Nolas, J. Mater. Chem. 18, 842 (2008).
- 17. G.B. Adams, M. O'Keefe, A.A. Demkov, O.F. Sankey and Y.-M. Huang, Phys. Rev. B **46**, 8048 (1994).
- 18. J.C. Conesa, C. Tablero and P. Wahnon, J. Chem. Phys. 120, 6142 (2004).
- 19. V.I. Smelyansky and J.S. Tse, Chem. Phys. Lett. 264, 459 (1997).
- 20. N.F. Mott, J. Solid State Chem. **6**, 348 (1973).
- 21. S.B. Roy, K.E. Sim and A.D. Caplan, Phil. Mag. B 65, 1445 (1992).
- 22. M. Beekman and G.S. Nolas, Physica B 383, 111 (2006).
- 23. M. Beekman, W. Schnelle, H. Borrmann, M. Baitinger, Yu. Gring and G.S. Nolas, Phys. Rev. Letter **104**, 018301 (2010).
- 24. J. Martin and G. S. Nolas, Rev. Sci. Instrum. 87, 015105 (2016).
- 25. B.C. Sales, B.C. Chakoumakos, D. Mandrus and J.W. Sharp, J. Solid State Chem. **146**, 528 (1999).
- 26. M.G. Alexander, D.P. Goshorn and D.G. Onn, Phys. Rev. B 22, 4535 (1980).
- 27. A. Tari, The Specific Heat of Matter at Low Temperatures, Imperial College Press (London), 2003.
- 28. X. Tang, J. Dong, P. Hutchins, O. Shebanova, J. Gryko, P. Barnes, J.K. Cockcroft, M. Vickers and P.F. McMillan, Phys. Rev. B **74**, 014109 (2006).
- 29. R.P. Hermann, W. Schweika, O. Leupold, R. Rüffer, G.S. Nolas, F. Grandjean and G.J. Long, Phys. Rev. B **72**, 174301 (2005).
- 30. G.S. Nolas, T.J.R. Weakley, J.L. Cohn and R. Sharma, Phys. Rev. B 61, 3845 (2000).
- 31. J.C. Conesa, C. Tablero and P. Wahnon, J. Chem. Phys. 120, 6142 (2004).
- 32. A. Bentien, V. Pacheco, S. Paschen, Yu. Grin and F. Steglich, Phys. Rev. B 71, 165206 (2005).
- 33. M.A. Avila, D. Huo, T. Sakata, K. Suekuni and T. Takabatake, J. Phys.: Condens. Matater **18**, 1585 (2006).
- 34. G.S. Nolas, M. Beekman, J. Gryko, G.A. Lamberton, Jr., T.M. Tritt and P.F. McMillan, Appl. Phys. Lett. **82**, 910 (2003).
- 35. S. Stefanoski, M. Beekman, W. Wong-Ng, P. Zavalij and G.S. Nolas, Chem. Mater. 23, 1491 (2011).
- 36. S. Stefanoski, J. Martin and G.S. Nolas, J. Phys.: Cond. Matter 22, 485404 (2010).
- 37. H. Morito, T. Yamada, T. Ikeda and H. Yamane, J. Alloys Comp. **480**, 723 (2009).
- 38. M. Beekman, R.P. Hermann, A. Mochel, F. Juranyi and G.S. Nolas, J. Phys.: Cond. Matter, **22**, 355401 (2010).
- 39. F. Brunet, P. Mélinon, A. San-Miguel, P. Kéghélian, A. Perez, A.M. Flank, E. Reny, C. Cros and M. Pouchard, Phys. Rev. B **61**, 16550 (2000).
- 40. A.D. Ritchie, M.A. MacDonald, P. Zhang, M.A. White, M. Beekman, J. Gryko and G.S. Nolas, Phys. Rev. B **82**, 155207 (2010).
- 41. H. Libotte, J.-P. Gaspard, A. San Miguel and P. Mélinon, Europhys. Lett. 64, 757 (2003).
- 42. S. Stefanoski, C.D. Malliakas, M.G. Kanatzidis and G.S. Nolas, Inorg. Chem. **51**, 8686 (2012).
- 43. V.I. Smelyanski and J.S. Tse, Chem. Phys. Lett. **264**, 459 (1997).
- 44. A. Demkov, O.F. Sankey, K.E. Schmidt, G.B. Adams and M. O'Keeffe, Phys. Rev. B **50**, 17001 (1994).

- 45. Y. Hasegawa, Y. Ling, S. Yamazaki, T. Hashizume, H. Shinohara, A. Sakai, H.W. Pickering and T. Sakurai, Phys. Rev. B **56**, 6470 (1997).
- 46. M. Beekman and G.S. Nolas, J. Mater. Chem. 18, 842 (2008).
- 47. S. Stefanoski and G.S. Nolas, Cryst. Growth Des. 11, 4533 (2011).
- 48. S. Stefanoski, M.C. Blosser and G.S. Nolas, Cryst. Growth Des. 13, 195 (2013).
- 49. M.C. Blosser and G.S. Nolas, Mater. Lett. **99**, 161 (2013).
- 50. A.M. Guloy, R. Ramlau, Z. Tang, W. Schnelle, M. Baitinger and Y. Grin, Nature 443, 320 (2006).
- 51. A.M. Guloy, R. Ramlau, Z. Tang, W. Schnelle, M. Baitinger and Y. Grin, Eur. J. Inorg. Chem. 17, 2455 (2009).
- 52. Y. Liang, B. Bohme, M. Reibold, W. Schnelle, U. Schwarz, M. Baitinger, H. Lichte and Y. Grin, Inorg. Chem. **50**, 4523 (2011).
- 53. B. Bohme, S. Hoffmann, M. Baitinger and Y. Grin, Z. Naturforsch 66b, 230 (2011).
- 54. Y. Dong, P. Chai, M. Beekman, X. Zeng, T. M. Tritt and G. S. Nolas, Inorg. Chem. **54**, 5316 (2015).
- 55. Y. He, F. Sui, S.M. Kauzlarich and G. Galli, Energy Environ. Sci. 7, 2598 (2014).
- 56. V. Baran, A. Senyshyn, A.J. Karttunen, A. Fischer, W. Scherer, G. Raudaschl-Sieber and T.F. Fässler, Chem. Eur. J. **20**, 1 (2014).
- 57. J.H. Roudebush, C.de la Cruz, B.C. Chakoumakos and S.M. Kauzlarich, Inorg. Chem. **51**, 1805 (2012).
- 58. R.D. Shannon, Acta Cryst. A 32, 751 (1976).
- 59. L. Krishna, P. Chai, C.A. Koh, E.S. Toberer and G.S. Nolas, Mater. Lett. 149, 123 (2015).
- 60. Y. Dong and G. S. Nolas, Cryst. Eng. Comm. 17, 2242 (2015).
- 61. K. Wei, Y. Dong and G. S. Nolas, J. Solid State Chem. 237, 81 (2016).
- 62. K. Wei, X. Zeng, T. M. Tritt, A. R. Khabibullin, L. M. Woods and G. S. Nolas, Mater. 9, 732 (2016).
- 63. B. Böhme, K. Wei, M. Bobnar, Y. Prots, U. Burkhard, M. Baitinger, G. S. Nolas and Y.
- Grin, Zeitschrift für Kristallographie, DOI: https://doi.org/10.1515/zkri-2017-2046 (2017).
- 64. Z. Ge, K. Wei and G. S. Nolas, Phys. Status Solidi A 210, 2725 (2013).
- 65. K. Wei, J. Martin and G.S. Nolas, Mater. Lett. 122, 289 (2014).
- 66. Z. Ge, K. Wei, H. Lewis, J. Martin and G. S. Nolas, J. Solid State Chem. 225, 354 (2015).
- 67.Y. Dong, A.R. Khabibullin, K. Wei, J.R. Salvador, G.S. Nolas and L.M. Woods, ChemPhysChem **16**, 3264 (2015).

Students and Postdocs that worked under this project

Students: Matt Beekman / Stevce Stefanoski / Micheal Blosser / Jagannath Paul / Robert Hyde / Marek Merlak / Devajyoti Mukherjee / Ted Wangensteen / Kaya Wei / Gayan Dedigamuwa Postdocs: Dr. Matt Beekman / Dr. Yongkwan Dong / Dr. Ping Chai / Dr. Zhenhua Ge / Dr. Stevce Stefanoski / Dr. Kaya Wei / Dr. Tara Dhakal / Dr. Vaithianathan Veeramuthu / Dr. Hasitha Weerasinghe

Publications under this project (46 journal articles, one book, and three book chapters)

- H. Zhang, H. Liu, K. Wei, O. Kurakevych, Y. L. Godec, Z. Liu, J. Martin, M. Guerrette, G. S. Nolas and T. A. Strobel, 'BC8 Silicon (Si-III) is a Narrow-Gap Semiconductor', Phys. Rev. Lett. 118, 146601 (2017).
- A. R. Khabibullin, T. D. Huan, G. S. Nolas and L. M. Woods, 'Cage disorder and gas encapsulation as routes to tailor properties of inorganic clathrates', Acta Mater. 131, 475 (2017).
- B. Böhme, K. Wei, M. Bobnar, Y. Prots, U. Burkhard, M. Baitinger, G. S. Nolas and Y. Grin, 'A type-II clathrate with a Li-Ge framework', Zeitschrift für Kristallographie, https://doi.org/10.1515/zkri-2017-2046 (2017).
- M. Beekman, K. Wei and G. S. Nolas, 'Clathrates and beyond: Low-density allotropy in crystalline silicon', Appl. Phys. Rev. 3, 040804 (2016).
- K. Wei, X. Zeng, T. M. Tritt, A. R. Khabibullin, L. M. Woods and G. S. Nolas, 'Structure and Transport Properties of Dense Polycrystalline Clathrate-II (K,Ba)₁₆(Ga,Sn)₁₃₆ Synthesized by a New Approach Employing SPS', Mater. 9, 732 (2016).
- I. Veremchuk, M. Beekman, I. Antonyshyn, W. Schnelle, M. Baitinger, G. S. Nolas and Y. Grin, 'Binary Alkali-Metal Silicon Clathrates by Spark Plasma Sintering: Preparation and Characterization', Mater. 9, 593 (2016).
- K. Wei, Y. Dong and G. S. Nolas, 'Precursor routes to quaternary intermetallics: Synthesis, crystal structure, and physical properties of clathrate-II Cs₈Na₁₆Al₂₄Si₁₁₂', J. Solid State Chem. 237, 81 (2016).
- M. Beekman, D.T. Morelli, and G.S. Nolas, 'Better thermoelectrics through glass-like crystals', Nature Materials 14, 1182 (2015).
- Y. Dong and G. S. Nolas, 'Crystal Growth through Field-Assisted Electrochemical Redox and Ion-Exchange Reactions: A Case Study of K_{4.2}Na_{3.8}Si₄₆ Clathrate-I', Cryst. Growth Des. 15, 4731 (2015).
- Y. Dong, A. R. Khabibullin, K. Wei, J. R. Salvador, G. S. Nolas and L. M. Woods, 'Bournonite PbCuSbS₃: Stereochemically Active Lone-Pair Electrons that Induce Low Thermal Conductivity', ChemPhysChem, 16, 3264 (2015).

- Y. Dong, P. Chai, M. Beekman, X. Zeng, T. M. Tritt and G. S. Nolas, 'Precursor Routes to Complex Ternary Intermetallics: Single-Crystal and Microcrystalline Preparation of Clathrate-I Na₈Al₈Si₃₈ from NaSi + NaAlSi', Inorg. Chem. 54, 5316 (2015).
- K. Wei and G. S. Nolas, 'Synthesis and Characterization of Nanostructured Stannite Cu₂ZnSnSe₄ and Ag₂ZnSnSe₄ for Thermoelectric Applications', ACS Appl. Mater. Interfaces 7, 9752 (2015).
- L. Krishna, P. Chai, C. A. Koh, E. S. Toberer, and G. S. Nolas, 'Synthesis and structural properties of type I potassium SiGe alloy clathrates', Mater. Lett. 149, 123 (2015).
- Y. Dong and G. S. Nolas, 'Rapid Crystal Growth of Type-II Clathrates A₈Na₁₆Si₁₃₆ (A = K, Rb, Cs) by Spark Plasma Sintering', Cryst. Eng. Comm. 17, 2242 (2015).
- Z. Ge, K. Wei, H. Lewis, J. Martin, and G. S. Nolas, 'Bottom-up processing and low temperature transport properties of polycrystalline SnSe', J. Solid State Chem. 225, 354 (2015).
- A. Biswas, S. Chandra, S. Stefanoski, J. S. Blazquez, J. J. Ipus, A. Conde, M. H. Phan, V. Franco, G. S. Nolas, and H. Srikanth, 'Enhanced cryogenic magnetocaloric effect in Eu₈Ga₁₆Ge₃₀clathrate nanocrystals', J. Appl. Phys. 117, 033903 (2015).
- G. S. Nolas, editor, The Physics and Chemistry of Inorganic Clathrates, Springer, 2014.
- M. Beekman and G. S. Nolas, 'Synthetic Approaches to Intermetallic Clathrates' in The Physics and Chemistry of Inorganic Clathrates, edited by G. S. Nolas, Springer-Verlag, 2014.
- S. Stefanoski, M. Beekman, and G. S. Nolas, 'Inorganic Clathrates for Thermoelectric Applications' in The Physics and Chemistry of Inorganic Clathrates, edited by G. S. Nolas, Springer-Verlag, 2014.
- S. Paschen, M. Ikeda, S. Stefanoski, and G. S. Nolas, 'Structural and Physical Properties of Rare-Earth Clathrates' in The Physics and Chemistry of Inorganic Clathrates, edited by G. S. Nolas, Springer-Verlag, 2014.
- H. J. Jakobsen, H. Bildsøe, M. Beekman, S. Stefanoski, G. S. Nolas, and C. R. Bowers, 'Low-Temperature ²³Na MAS NMR Reveals Dynamic Effects and Compositions for the Large and Small Channels in the Zeolite-Like Ge-Framework of Na_{1-x}Ge_{3+z} Materials', J. Phys. Chem.118, 28890 (2014).
- K. Wei, J. Martin, and G. S. Nolas, 'Synthesis, SPS processing and low temperature transport properties of polycrystalline FeSb₂ with nano-scale grains', Mater. Lett. 122, 289 (2014).
- Z. Ge, K. Wei, and G. S. Nolas, 'Synthesis and low-temperature transport properties of polycrystalline NiSe₂', Phys. Status Solidi A 210, 2725 (2013).

- A. D. Ritchie, M. B. Johnson, J. F. Niven, M. Beekman, G. S. Nolas, J. Gryko, and M. A. White, 'Influence of guest loading on thermal properties of Na_xSi₁₃₆ clathrates', J. Phys. Cond. Matter 25, 435401 (2013).
- S. Stefanoski, Y. Dong, and G. S. Nolas, 'Structural characterization and low-temperature physical properties of p-type single-crystal K₈Ga_{8.5}Sn_{37.5} grown by self-flux method', J. Solid State Chem. 204, 166 (2013).
- M. C. Blosser and G. S. Nolas, 'Synthesis of Na₈Si₄₆ and Na₂₄Si₁₃₆ by oxidation of Na₄Si₄ from ionic liquid decomposition', Mater. Lett. 99, 161 (2013).
- S. Stefanoski, M. C. Blosser, and G. S. Nolas, 'Pressure Effects on the Size of Type-I and Type-II Si-Clathrates Synthesized by Spark Plasma Sintering', Cryst. Growth Des. 13, 195 (2013).
- A.N. Mansour, J. Martin, W. Wong-Ng, and G. S. Nolas, 'Electronic and atomic structure of Ba₈Ga₁₆Ge_{30-x}Si_x type I clathrates: Ge and Ga XAFS study', J. Phys. Cond. Matter 24, 485503 (2012).
- S. Stefanoski, C. D. Malliakas, M. G. Kanatzidis, and G. S. Nolas, 'Synthesis and Structural Characterization of Na_xSi_{136} ($0 < x \le 24$) Single Crystals and Low-Temperature Transport of Polycrystalline Specimens', Inorg. Chem. 51, 8686 (2012).
- S. Stefanoski and G. S. Nolas, 'Synthesis and Structural Characterization of Single-Crystal K_{7.5}Si₄₆ and K_{17.8}Si₁₃₆ Clathrates', Cryst. Growth Des. 11, 4533 (2011).
- S. Stefanoski, M. Beekman, W. Wong-Ng, P. Zavalij, and G. S. Nolas, 'Simple approach for selective crystal growth of intermetallic clathrates', Chem. Mater. 23, 1491 (2011).
- S. Stefanoski, J. Martin and G.S. Nolas, 'Low temperature transport properties and heat capacity of single-crystal Na₈Si₄₆', J. Phys. Cond. Matter 22, 485404 (2010).
- A.D. Ritchie, M.A. MacDonald, P. Zhang, M.A. White, M. Beekman, J. Gryko and G.S. Nolas, 'X-ray absorption spectroscopy studies of local structure and electronic properties of Na_xSi₁₃₆ clathrates', Phys. Rev. B. 82, 155207 (2010).
- M. Beekman, R.P. Hermann, A. Mochel, F. Juranyi and G.S. Nolas, 'A Study of low-energy Na phonon modes in clathrate-II Na_xSi₁₃₆ (x=3, 23 and 24)', J. Phys. Cond. Matter 22, 355401 (2010).
- M. Beekman, E.N. Nenghabi, K. Biswas, C.W. Myles, M. Baitinger, Y. Grin and G.S. Nolas, 'Framework contraction in Na-stuffed Si(cF136)', Inorg. Chem. 49, 5338 (2010).
- M. Beekman, S. Stefanoski, W. Wong-Ng, J.A. Kaduk, Q. Huang, C. Reeg, C.R. Bowers and G.S. Nolas, 'Structure and thermal conductivity of Na_{1-x}Ge_{3+z}', J. Solid State Chem. 183, 1272 (2010).

- M. Beekman, W. Schnelle, H. Borrmann, M. Baitinger, Yu. Grin and G.S. Nolas, 'Intrinsic Electrical and Thermal Properties od Single Crystals of Na₂₄Si₁₃₆', Phys. Rev. Lett. 104, 018301 (2010).
- M. Beekman, M. Baitinger, H. Borrman, W. Schnelle, K. Meier, G.S. Nolas and Y. Grin, 'Preparation and crystal growth of Na₂₄Si₁₃₆', J. Am. Chem. Soc., 131, 9642 (2009).
- M. Beekman, J.A. Kaduk, J. Gryko, W. Wong-Ng and G. S. Nolas, 'Synthesis and Characterization of Framework-Substituted Cs₈Na₁₆Cu₅Ge₁₃₁ Type II Clathrate,' J. of Alloys and Comp. 470, 365 (2009).
- A.N. Mansour, M. Beekman, W. Wong-Ng and G.S. Nolas, 'Local Structure of Cu in Cs8Na₁₆Cu₅Ge₁₃₁ Type II Clathrate,' J. of Solid State Chem. 182, 107 (2009).
- K. Biswas, C.W. Myles, M. Sanati and G.S. Nolas, 'Thermal Properties of Guest-free Si₁₃₆ and Ge₁₃₆ Clathrates: A First Principles Study, 'J. Appl. Phys. 104, 033535 (2008).
- J. Martin, H. Wang and G.S. Nolas, 'Optimization of the Thermoelectric Properties of Ba₈Ga₁₆Ge₃₀,' Appl. Phys. Lett. 92, 222110 (2008).
- M. Beekman and G.S. Nolas, 'Inorganic clathrate-II materials of group 14: synthetic routes and physical properties,' J. Mater. Chem. 18, 842 (2008).
- J. Martin, G.S. Nolas, H. Wang and J. Yang, 'Thermoelectric properties of silicon-germanium type I clathrates,' J. Appl. Phys. 102, 103719 (2007).
- C.L. Condron, S.M. Kauzlarich and G.S. Nolas, 'Structure and Thermoelectric Characterization of $A_xBa_{8-x}Al_{14}Si_{31}$ (A = Sr, Eu) Single Crystals,' Inorg. Chem. 46, 2556 (2007).
- M. Beekman, W. Wong-Ng, J.A. Kaduk, A. Shapiro and G.S. Nolas, 'Synthesis and single-crystal X-ray diffraction studies of new framework substituted type II clathrates, $Cs_8Na_{16}Ag_xGe_{136-x}$ (x < 7),' J. Solid State Chem. 180, 1086 (2007).
- C.L. Condron, J. Martin, G.S. Nolas, P.M.B. Piccoli, A.J. Schultz and S.M. Kauzlarich, 'Structure and Thermoelectric Characterization of Ba₈Al₁₄Si₃₁,' Inorg. Chem. 45, 9381 (2006).
- M. Beekman and G.S. Nolas, 'Synthesis and thermal conductivity of type II silicon clathrates,' Physica B 383, 111 (2006).
- R.P. Hermann, V. Keppens, P. Bonville, G.S. Nolas, F. Grandjean, G.J. Long, H.M. Christen, B.C. Chakoumakos, B.C. Sales and D. Mandrus, 'Direct Experimental Evidence for Atomic Tunneling of Europium in Crystalline Eu₈Ga₁₆Ge₃₀,' Phys. Rev. Lett. 97, 017401 (2006).
- F. Chen, J. Shulman, Y. Xue, C.W. Chu and G.S. Nolas, 'Thermal conductivity measurement under hydrostatic pressure using the 3ω method,' Rev. Sci. Intsr. 75, 4578 (2004).

Patents Under This Grant

M. Beekman and G. S. Nolas, 'Novel Methods for Solid State Crystal Growth', US Patent 8,414,858, April 9, 2013.

G. S. Nolas, S. Witanachchi and P. Mukherjee, 'Method of Manufacturing a Clathrate Compounds', US Patent 8,211,400, July 3, 2012.